FACETS

FP6-2004-IST-FETPI 15879

Fast Analog Computing with Emergent Transient States

D16

Progress report on model developments and comparison to experimental data

Report Version: Final

Report Preparation: A. Destexhe (UNIC) and A. Lansner (KTH)

Classification: Public

Contract Start Date: 01/09/2005 Duration: 4 Years

Project Co-ordinator: Karlheinz Meier (Heidelberg)

Partners: U Bordeaux, CNRS (Gif-sur-Yvette, Marseille), U Debrecen, TU Dresden, U Freiburg, TU Graz, U Heidelberg, EPFL Lausanne, Funetics S.a.r.l., U London, U Plymouth, INRIA, KTH Stockholm

Project funded by the European Community

under the "Information Society Technologies' Programme

DELIVERABLE SUMMARY SHEET

Project Number: FP6-2004-IST-FETPI 15879

Project Acronym: FACETS

Title: Fast Analog Computing with Emergent Transient States

Deliverable N°: D16
Due date: 02-2007
Delivery Date: 03-2007

Short Description:

This deliverable reports on network model developement under FACETS during the first 18 months. It is divided in two parts, which correspond to the main streams of WP5. In the first part, we review the development of "generic" network models of active cortical states in cerebral cortex based on in vivo data. The properties of "active states" (such as in waking animals) are reviewed, both for cellular and network properties. Different types of models are then overviewed, and these models are compared to experimental data. They form the seed for the next generation of FACETS models. In the second part, we overview the present status of the development of models of the primary visual system pathway (retina, thalamus, primary visual cortex or V1). Different models are outlined, as well as some of their features, while a detailed description of the V1 model properties is reported in another deliverable (D25, "Model for a hypercolumn in V1").

Partner owning: UNIC, KTH

Partners contributed: UNIC, KTH, ALUF, TUG, UHEI, INCM, UOP

Made available to: Public

Contents

List of Figures

Introduction

This report is divided in two parts, generic models of "active" states in cortex (Section 1), and models of primary visual cortex (V1; Section 2). These two parts correspond, respectively to Task 2 and Task 3 of the workpackage devoted to network models (WP5) in FACETS.

In both parts, we overview the "first generation" of network models developed in FACETS. The consortium of modeling groups in FACETS has an impressive diversity, from detailed biophysically-based models, to simplifed rate-based (non spiking) models. So as a first step towards a full integration of all these modeling efforts into a common goal, we have studied common problems by keeping the diversity of modeling approaches. These studies result in what we call the "first generation" of network models, which is reported here. The common goals of this first generation correspond to the two main sections of this report, and concern the genesis of active states, and the building of models of the primary visual pathway.

1

Generic models of active cortical states

We start this first part on generic models by summarizing measurements of cellular and network activities during active cortical states. Next, we overview the structure of the different models presently developed within FACETS. The last section is devoted to the comparison of models to experimental data.

1.1 Summary of experimental data

The term "active state" refers to cortical activity in states of vigilance corresponding to the awake animal. The electroencephalogram (EEG) during such active states is typically "desynchronized", i.e., of low amplitude and irregular activity dominated by fast frequencies (15-60 Hz; see Fig. 1.1, Awake, EEG). Intracellularly, neurons are depolarized and fire tonic and irregular discharges (Fig. 1.1, Awake, Intra). This level of irregularity is also apparent in multiunit activity (Fig. 1.1, Awake, Units). During slow-wave sleep (SWS), the activity consists in UP and DOWN states which are in register with EEG slow waves (Fig. 1.1, SWS). Locally, the UP states are associated with desynchronized EEG, and thus can be considered as network states very close to active states. Indeed, network activity is very similar during UP states compared to wakefulness (Fig. 1.1, SWS, Units). This similarity extends to various measurements, such as the patterns of discharges, patterns of correlation and relations between EEG and unit activity (Destexhe et al., 1999).

Note that, in contrast to the "global" UP states observed in vivo, "local" UP states have also been observed in vitro (Cossart et al., 2003). In this case, only a subset of the neurons enter simultaneously into firing activity. These local UP states have been connected to attractor dynamics and give additional constraints on dwell time and on activity levels. They last for several hundred milliseconds and include about 0.5-2% of the population. In the models reviewed here, we will consider sustained active states (as in waking animals), as well as global and local UP states.

Active states were characterized experimentally both from extracellular and intracellular recordings in order to provide constraints for models. The first type of characterization are the statistics of firing rates (Fig. 1.2A). During wakefulness, there is a large diversity of spontaneous firing rates in different cells with inhibitory cells having larger rates of discharge (around 30 Hz on average) compared to excitatory cells (around 10 Hz on average). The interspike interval distributions computed from single cells are exponentially distributed as for Poisson stochastic processes (Fig. 1.2B). Avalanche analysis was also performed (Bedard et al., 2006) and did not reveal the typical power-law scaling behavior of critical states, but rather exponential distributions (Fig. 1.2C), compatible with the Poisson statistics of single-cell firing patterns. Finally, conductance measurements were performed from intracellular recordings (Rudolph et al., 2007). Such measurements also revealed a large diversity in different cells. Plotting the relative conductance (absolute conductance divided by the leak conductance) revealed that excitation is on average around 1, while inhibition is larger, around 1.5 on average (Fig. 1.2D).

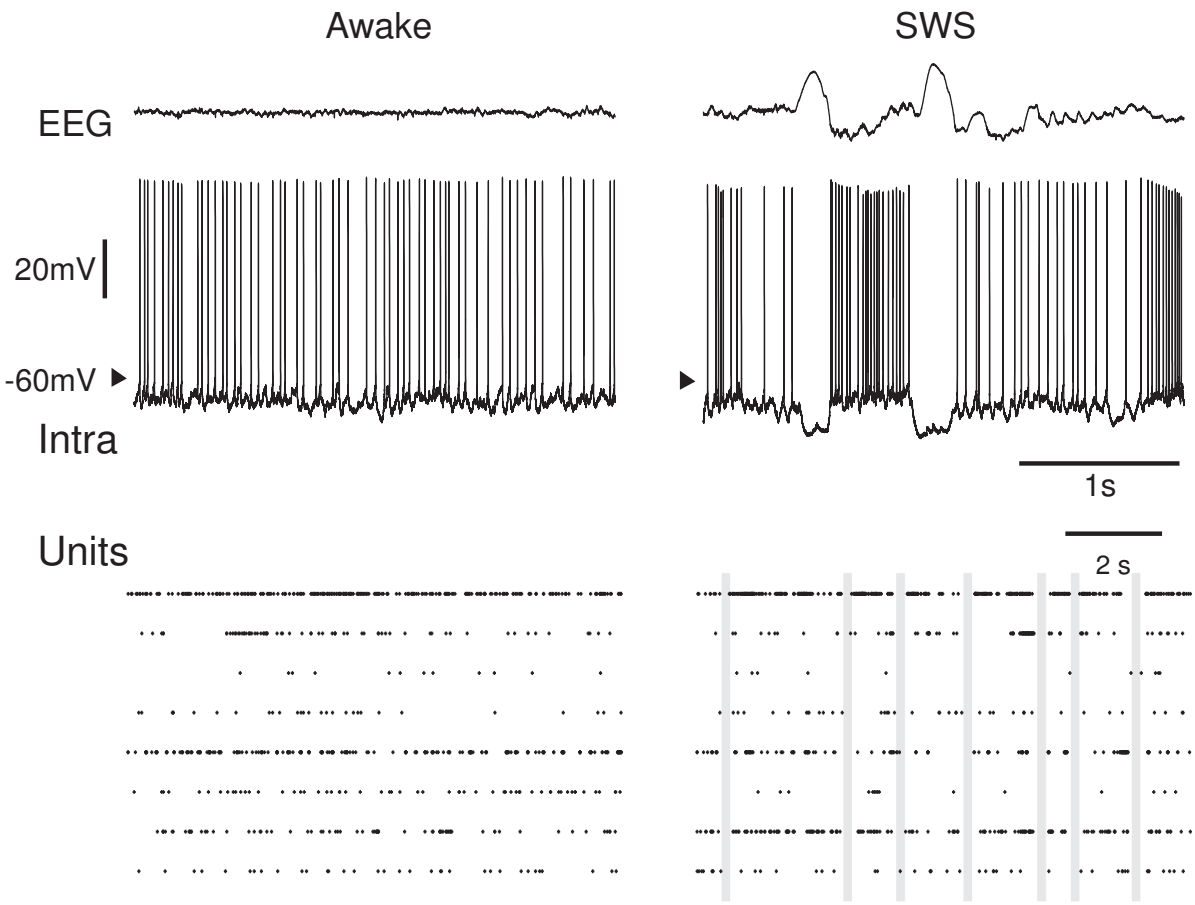

Figure 1.1. Cortical activity during active states and up/down states during slow-wave sleep.
Top traces: EEG and intracellular activity during wakefulness (left) and slow-wave sleep (right; modified from Steriade et al., 2001). Bottom traces: raster plots of multiunit spiking activity at 8 extracellular electrodes (modified from Destexhe et al., 1999). During SWS, the DOWN states are indicated by vertical gray bars. All recordings were obtained from cat association cortex (area 5-7).

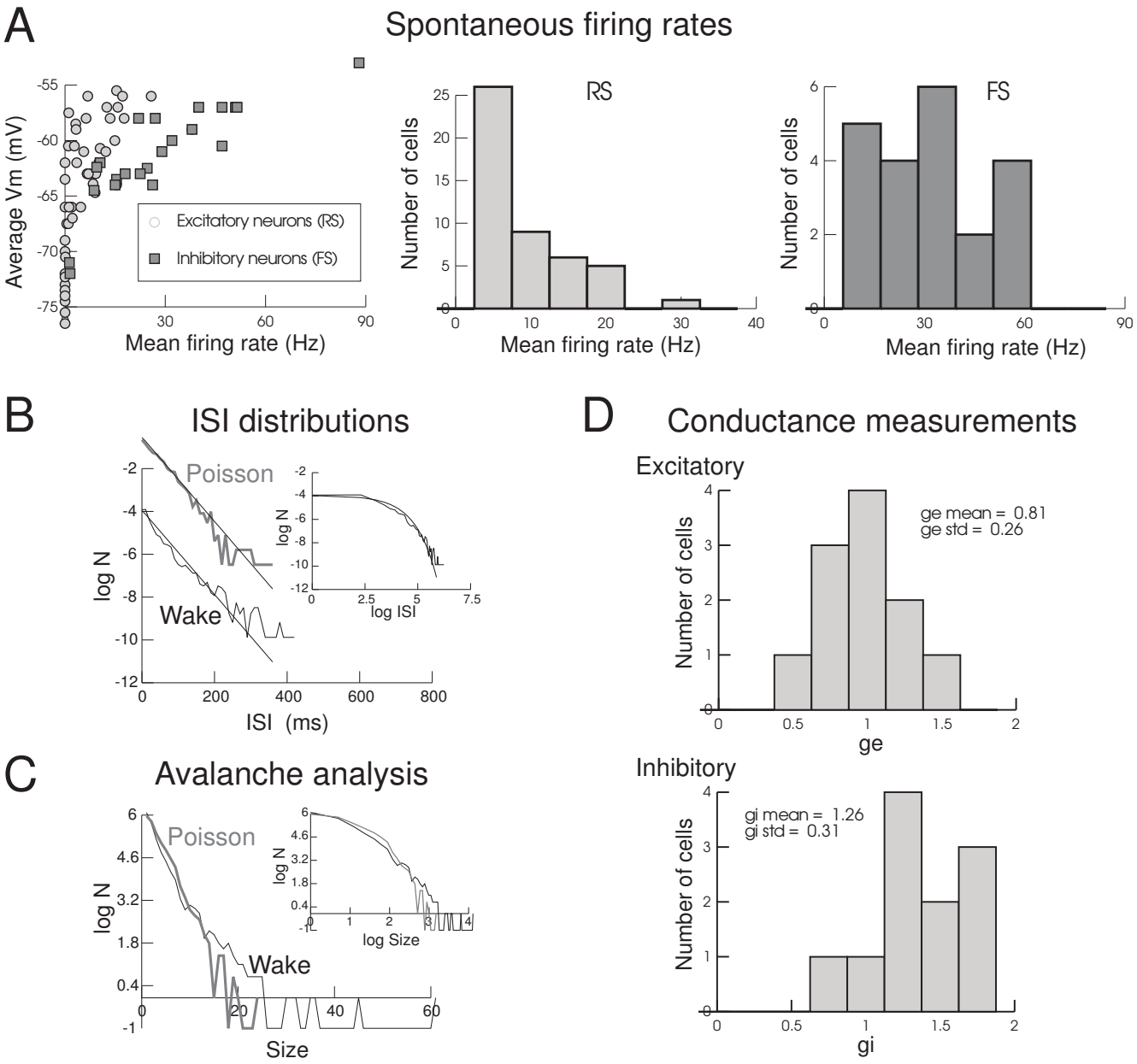

Figure 1.2. Analysis of cortical activity during active states.
A. Statistics of firing rates during wakefulness in cats. The left panel shows the relationship between the average V_m and the firing rate of different excitatory and inhibitory cells during wakefulness. The middle panel shows the distribution of firing rates obtained for presumed excitatory neurons, while that of inhibitory neurons is shown in the right panel. B. Interspike interval (ISI) distributions computed from extracellularly recorded neurons in wakefulness. C. Avalanche analysis of extracellular recordings in the awake cat. D. Conductance measurements in awake cat. The distribution of relative excitatory (top) and inhibitory conductances (bottom) measured from intracellular recordings. Modified from Bedard et al., 2006 (B,C); Rudolph et al., 2007 (A,D).

1.2 Single-cell model of active states

The first type of model was directly linked to experimental data and was aimed at evaluating the plausibility of conductance measurements. The conductance measurements during wakefulness (Fig. 1.2D) were integrated into a single-compartment model with Hodgkin-Huxley kinetics (Rudolph et al., 2007). Integrating these measured values of conductances led the model to generate V_m activity in excellent agreement with the intracellular recordings (Fig. 1.3, Awake). Similarly, integrating conductance measurements during UP states (not shown) generated V_m activity consistent with the UP-DOWN state transitions seen experimentally (Fig. 1.3, SWS). These results show that the conductance estimates are consistent with the V_m activity recorded experimentally during active states.

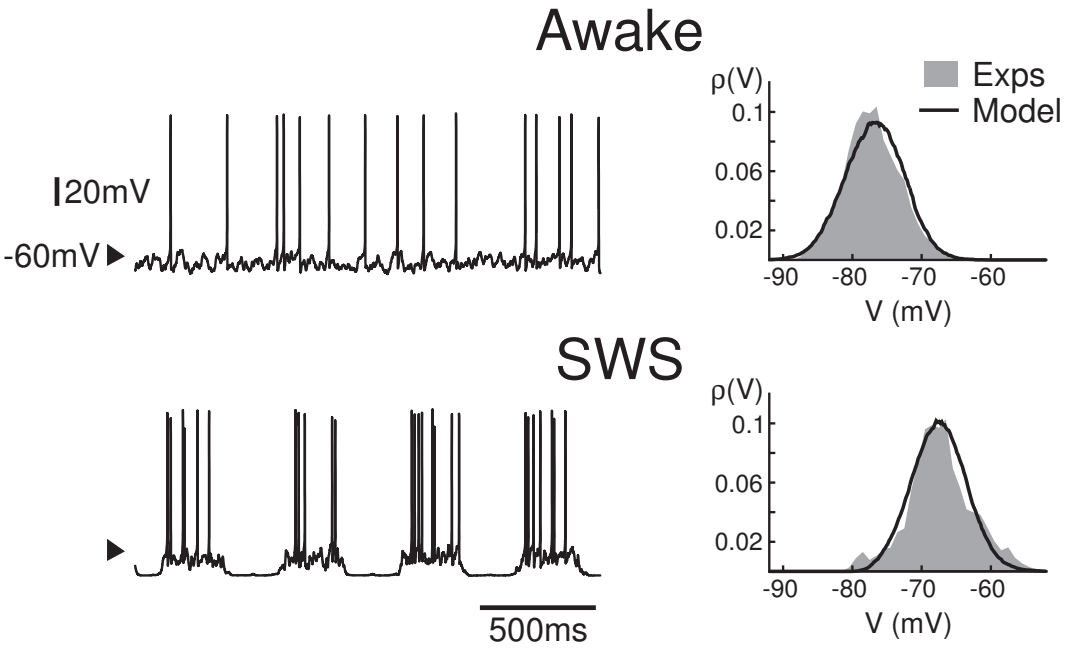

Figure 1.3. Hodgkin-Huxley model of cortical activity during active states and UP/DOWN states. Top: simulated intracellular activity corresponding to measurements in the wake state (based on conductance values shown in Fig. 1.2D). Bottom: simulated UP and DOWN states transitions during slow-wave sleep (based on the values given in Rudolph et al., 2007). Right panels: V_m distributions obtained in the model (solid lines) compared to that of the experiments (gray) in the same conditions (DC injection of -0.5 and -0.43 nA, respectively). Note that the distribution in bottom right panel was caculated only from UP states. Modified from Rudolph et al., 2007.

1.3 Network models of active states

In this section, we describe successively different types of generic models of active states. These models range from medium-scale (Model 1, Section 1.3.1) and large-scale networks (Model 2, Section 1.3.2) exhibiting self-sustained active states, small-scale networks exhibiting active states but with external noisy input (Models 3 and 4; Sections 1.3.3 and 1.3.4), and very-large scale networks exhibiting local UP states with attractor dynamics (Model 5; Section 1.3.5). Each model is described below, while the comparison with experimental data is reported in Section 1.4.

1.3.1 Model 1: Medium-scale generic network model of active states

The first type of model (Model 1), developed at UNIC, consisted in networks of spiking neurons with conductance-based synapses. The model consisted in 4,000 neurons, which were separated into two populations of excitatory and inhibitory neurons, forming 80% and 20% of the neurons, respectively. All neurons were connected randomly using a connection probability of 2%.

The membrane equation of all models was given by:

$$C_m \frac{dV}{dt} = -g_L(V - E_L) + S(t) + G(t) , \tag{1.1}$$

where $C_m = 1$ μF/cm^2 is the specific capacitance, V is the membrane potential, $g_L = 5{\times}10^{-5}$ S/cm^2 is the leak conductance density and E_L = -60 mV is the leak reversal potential. Together with a cell area of 20,000 μm^2, these parameters give a resting membrane time constant of 20 ms and an input resistance at rest of 100 MΩ. The function $S(t)$ represents the spiking mechanism and $G(t)$ stands for synaptic interactions (see below).

Integrate and Fire (IF) models

In addition to passive membrane properties, IF neurons had a firing threshold of -50 mV. Once the Vm reaches threshold, a spike is emitted and the membrane potential is reset to -60 mV and remains at that value for a refractory period of 5 ms. This model was inspired from a previous publication reporting self-sustained irregular states (Vogels and Abbott, 2005).

Hodgkin-Huxley (HH) models

HH neurons were modified from Traub and Miles (1991) and were described by the following equations:

$$\begin{aligned} C_m \frac{dV}{dt} &= -g_L(V - E_L) - \bar{g}_{Na}\, m^3 h\, (V - E_{Na}) - \bar{g}_{Kd}\, n^4\, (V - E_K) + G(t) \\ \frac{dm}{dt} &= \alpha_m(V)\,(1 - m) - \beta_m(V)\, m \\ \frac{dh}{dt} &= \alpha_h(V)\,(1 - h) - \beta_h(V)\, h \\ \frac{dn}{dt} &= \alpha_n(V)\,(1 - n) - \beta_n(V)\, n , \end{aligned} \tag{1.2}$$

where $\bar{g}_{Na} = 100\ mS/cm^2$ and $\bar{g}_{Kd} = 30\ mS/cm^2$ are the maximal conductances of the sodium current and delayed rectifier with reversal potentials of $E_{Na} = 50\ mV$ and $E_K = -90\ mV$. m, h, and n are the activation variables which time evolution depends on the voltage-dependent rate constants α_m, β_m, α_h, β_h, α_n and β_n. The voltage-dependent expressions of the rate constants were modified from the model described by Traub and Miles (1991):

$$
\begin{aligned}
\alpha_m &= 0.32 * (13 - V + V_T)/[\exp((13 - V + V_T)/4) - 1] \\
\beta_m &= 0.28 * (V - V_T - 40)/[\exp((V - V_T - 40)/5) - 1] \\
\alpha_h &= 0.128 * \exp((17 - V + V_T)/18) \\
\beta_h &= 4/[1 + \exp((40 - V + V_T)/5)] \\
\alpha_n &= 0.032 * (15 - V + V_T)/[\exp((15 - V + V_T)/5) - 1] \\
\beta_n &= 0.5 * \exp((10 - V + V_T)/40) \ ,
\end{aligned}
$$

where V_T = -63 mV adjusts the threshold (which was around -50 mV for the above parameters).

Synaptic interactions

Synaptic interactions were conductance-based, according to the following membrane equation for neuron i:

$$C_m \frac{dV_i}{dt} = -g_L(V_i - E_L) + S(t) - \sum_j g_{ji}(t)(V_i - E_j) \ , \tag{1.3}$$

where V_i is the membrane potential of neuron i, $g_{ji}(t)$ is the synaptic conductance of the synapse from neuron j to neuron i, and E_j is the reversal potential of that synapse. E_j was of 0 mV for excitatory synapses, or -80 mV for inhibitory synapses.

Synaptic interactions were implemented as follows: when a spike occurred in neuron j, the synaptic conductance g_{ji} was instantaneously incremented by a quantum value (6 nS and 67 nS for excitatory and inhibitory synapses, respectively) and decayed exponentially with a time constant of 5 ms and 10 ms for excitation and inhibition, respectively.

Behavior of the models

These two types of models simulate a self-sustained irregular state of activity, in which all cells fire irregularly and are characterized by important subthreshold voltage fluctuations (Fig. 1.4). The similarity of activity in both IF and HH models shows that the spiking mechanism is not critical, and suggests that the irregular activity is due to the sparse connectivity in this model.

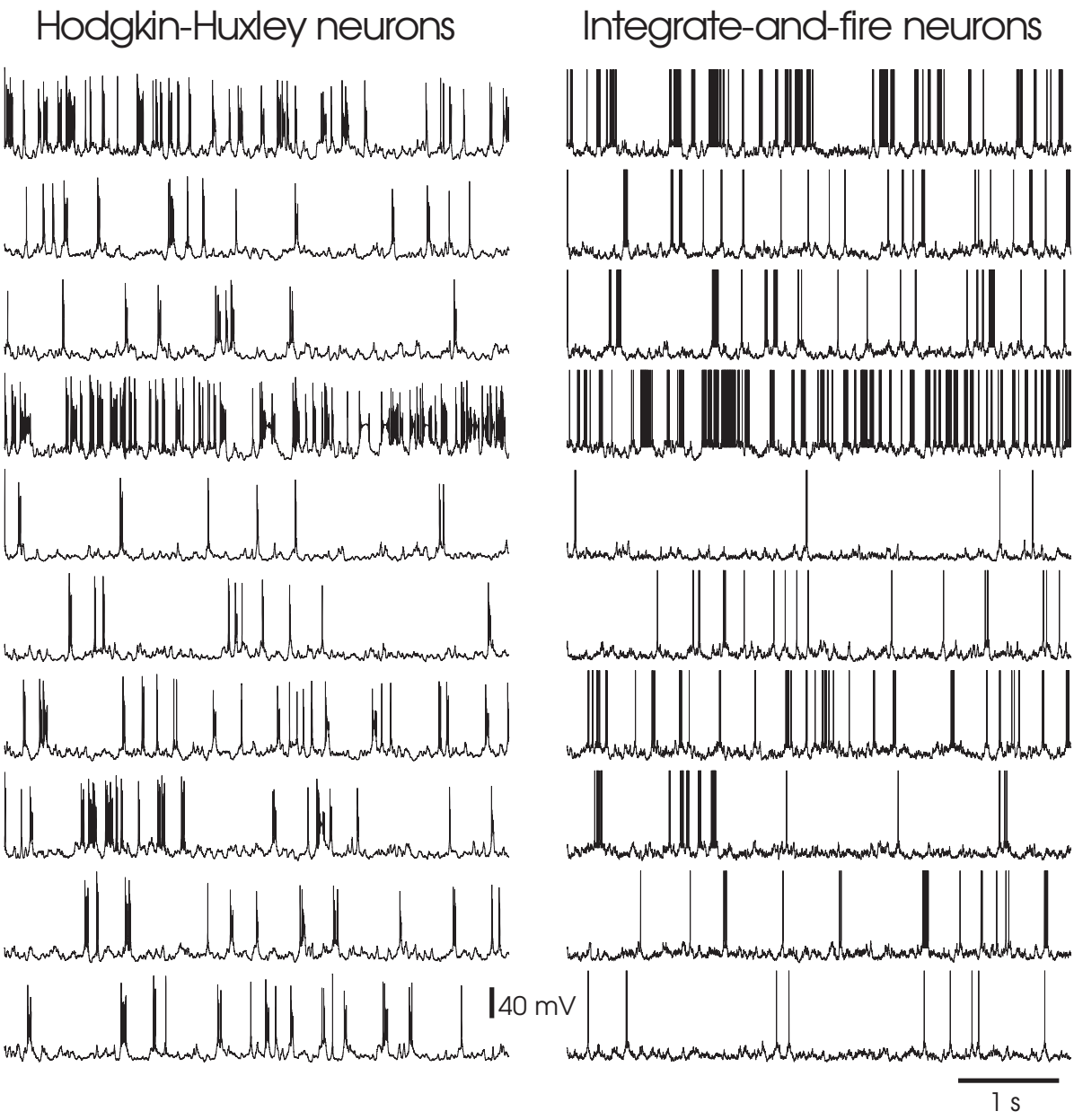

Figure 1.4. Model of active states (Model 1).
Two different network models are compared, and for each the activity of 10 cells randomly chosen in the network is displayed. Left: HH model, Right: IF model (see text for details). The two networks had the same (random) connectivity and the same 10 cells are shown. All simulations were run under the NEURON simulation environment (Hines and Carnevale, 1997).

1.3.2 Model 2: Large-scale generic network model of active states

In a second model study developed by ALUF (Kumar et al., 2007), we analyzed the dynamics of large recurrent random networks of integrate-and-fire neurons. We fixed the size of the networks at $N = 50{,}000$ for most simulations, but networks of up to 350,000 neurons were also considered in this study. We assumed that the larger fraction of all neurons ($N_{\text{exc}} = 0.8\,N$) were excitatory and the rest ($N_{\text{inh}} = 0.2\,N$) inhibitory. Each neuron received input from K neurons from within the network, of which $K_{\text{exc}} = 0.8\,K$ were randomly chosen from the excitatory pool, and $K_{\text{inh}} = 0.2\,K$ from the inhibitory pool. Multiple synapses between the same pair of neurons were allowed. The resulting networks were of relatively sparse connectivity, such that K/N was 0.1 or lower. In addition to the recurrent connections, each neuron received K_{ext} external Poisson-type inputs, all excitatory, with a rate ν_{ext} for each afferent. excitatory and inhibitory neurons were treated identically (Figure 1.5).

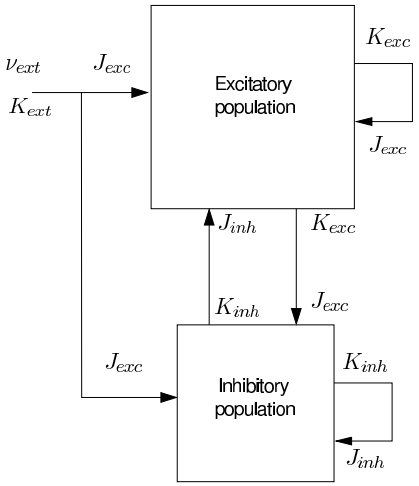

Figure 1.5. Network architecture for Model 2.
Two populations of N_{exc} excitatory and N_{inh} inhibitory neurons were sparsely connected in a recurrent fashion. Each neuron received input from K_{exc} excitatory and K_{inh} inhibitory neurons within the network. In addition, all neurons had K_{ext} excitatory connections representing non-local inputs to the network. The relative strength of inhibitory synapses g and the intensity of external inputs ν_{ext} were the control variables in numerical simulations of network dynamics.

The networks consisted of point neurons of the integrate-and-fire type. The I&F neuron model is computationally simple (Tuckwell, 1988a; Gerstner and Kistler, 2002) while known to capture essential features of input integration and spiking dynamics in real neurons (Rauch et al., 2003). For this neuron model, the subthreshold dynamics of the membrane potential $V^i(t)$ in neuron i is described by the leaky-integrator equation

$$C\,\frac{d}{dt}V^i(t) + G_{\text{rest}}\left[V^i(t) - V_{\text{rest}}\right] = I^i_{\text{syn}} \tag{1.4}$$

where I^i_{syn} is the total synaptic input current into neuron i. The resting potential was set to $V_{\text{rest}} = -70\,\text{mV}$. The parameters $C = 250\,\text{pF}$ and $G_{\text{rest}} = 16{,}7\,\text{nS}$ lead to a membrane time constant of $\tau_{\text{rest}} = C/G_{\text{rest}} = 15\,\text{ms}$, reflecting the electrical properties of the neuronal membrane in absence of any synaptic input. We implemented a deterministic threshold/reset mechanism for spike generation (Tuckwell, 1988a, 1988b), assuming a fixed spike threshold of 20 mV above rest ($V_\theta = -50\,\text{mV}$). After the membrane potential reached threshold, a spike was emitted, the membrane potential was reset to its resting value, and synaptic integration was halted for 2 ms mimicking the refractory period in real neurons.

In this study, synaptic input was modeled by transient conductance changes, using alpha-functions (Jack et al., 1975; Rotter et al., 1999a)

$$G(t) = \begin{cases} J\,\frac{t}{\tau}\,e^{1-\frac{t}{\tau}} & \text{for } t \geq 0 \\ 0 & \text{for } t < 0. \end{cases} \tag{1.5}$$

We refer to the peak amplitude J of the conductance transient, which is assumed at $t = \tau$ after onset, as the 'strength' of the synapse. Generally, excitatory and inhibitory synapses had different strengths J_{exc} and J_{inh} assigned. Both excitatory and inhibitory synapses, however, had in general identical time constants of $\tau_{\text{exc}} = \tau_{\text{inh}} = 0.326\,\text{ms}$. This value was obtained by fitting EPSPs with alpha-shaped EPSCs to the parameters of empirical

EPSPs, assuming a membrane time constant of 10 ms. This yielded rise times (time to peak) of about 1.7 ms, and a half width at half height of about 8.5 ms for EPSPs at rest. These values were close to what was reported from acute slices of cat visual cortex (Fetz et al., 1991). To explore the impact of this parameter for network dynamics, most simulations were repeated for $\tau_{\mathsf{exc}} = \tau_{\mathsf{inh}} = 0.978\,\mathrm{ms}$ (3-fold slower) and 1.63 ms (5-fold slower). For certain questions, we also employed combinations of different time constants for excitation and inhibition in our simulations.

The total excitatory conductance $G^i_{\mathsf{exc}}(t)$ in neuron i was given by

$$G^i_{\mathsf{exc}}(t) = \sum_{j=1}^{K_{\mathsf{exc}}+K_{\mathsf{ext}}} \sum_k G_{\mathsf{exc}}(t - t^j_k - D). \tag{1.6}$$

The outer sum runs over all excitatory synapses onto this particular neuron, the inner sum runs over the sequence of spikes arriving at a particular synapse. Similarly, the total inhibitory conductance $G^i_{\mathsf{inh}}(t)$ in neuron i was given by

$$G^i_{\mathsf{inh}}(t) = \sum_{j=1}^{K_{\mathsf{inh}}} \sum_k G_{\mathsf{inh}}(t - t^j_k - D). \tag{1.7}$$

A uniform transmission delay of $D = 1.5\,\mathrm{ms}$ was imposed for all synapses, in all simulations. The total synaptic current into neuron i was

$$I^i_{\mathsf{syn}}(t) = -G^i_{\mathsf{exc}}(t)\left[V^i(t) - V_{\mathsf{exc}}\right] - G^i_{\mathsf{inh}}(t)\left[V^i(t) - V_{\mathsf{inh}}\right], \tag{1.8}$$

where $V_{\mathsf{exc}} = 0\,\mathrm{mV}$ and $V_{\mathsf{inh}} = -80\,\mathrm{mV}$ are the reversal potentials of the excitatory and the inhibitory synaptic currents, respectively. The ratio

$$g = \frac{J_{\mathsf{inh}}\,\tau_{\mathsf{inh}}\,|V_{\mathsf{rest}} - V_{\mathsf{inh}}|}{J_{\mathsf{exc}}\,\tau_{\mathsf{exc}}\,|V_{\mathsf{rest}} - V_{\mathsf{exc}}|} \tag{1.9}$$

was used to parameterize the relative strength of effective inhibition. For fast conductance transients and small amplitudes, it corresponds approximately to the ratio of IPSP and EPSP peak amplitudes at rest. It is important to point out, however, that the inhibition/excitation ratio g (which was originally introduced for current based models) has a slightly different meaning for the conductance based synapse model. Being a quotient of peak potentials in previous work (Brunel, 2000), here g is approximately the ratio of total charges induced at rest.

It should also be noted that in the case of conductance based synapses, the effective time constant of the neuron depends on the input and can strongly deviate from the membrane time constant $\tau_0 = C/G_{\mathsf{rest}}$ without input (Kuhn et al., 2004). Active synapses contribute to the total membrane conductance, thereby also changing the membrane time constant. In this way, the integrative properties of the neuron depend on its input, and the model becomes nonlinear. This effect is not present in models where synapses are modeled as current sources.

Self-sustained activity in recurrent networks

From anatomical studies it is known that the number of sensory input fibers is very small compared to the number of neurons in the cortex, not to speak of the number of cortico-cortical connections (Braitenberg and Schüz, 1998). In fact, real-time optical imaging and single-unit recordings in the cat visual cortex *in vivo* showed that there is considerable, spatially organized activity even in the absence of a visual stimulus (Arieli et al., 1996). The neurons involved in such ongoing activity fire action potentials at relatively low rates (< 5 spikes/s) (Abeles, 1991; Latham et al., 2000; Chiu and Weliky, 2001). This activity component has been termed 'ongoing' activity, expressing that it presumably reflects dynamic brain processes beyond the direct effect of a sensory stimulus. Also isolated brain tissue, however, such as cortical cultures (Plenz and Aertsen, 1996) or deafferented cortical slabs (Burns and Webb, 1979; Timofeev et al., 2000), were found to be able to retain some spiking activity. Although it is well possible that 'spontaneously' active neurons (e.g. pacemaker cells in the thalamus) initiate activity in the otherwise silent cortex (Latham et al., 2000), it is nevertheless an interesting question whether cortical networks can also maintain stable spiking at low rates by means of their massive recurrent connections (Amit and Brunel, 1997; Salinas, 2003; Shu et al., 2003). For theoretical reasons, derived from the analysis of simple firing rate models, it has been claimed that stable self-sustained activity within the AI regime is impossible (Latham et al., 2000). Recently, however, the question was raised whether conductance based networks can behave differently (Kuhn et al., 2004; Schrader et al., 2005; Kumar et al., 2005; Vogels and Abbott, 2005). In particular, Kuhn et al. (2004) observed that neurons with synaptic conductances exhibited a non-monotonic response characteristic when driven by balanced input. They speculated that, for suitable network architectures, this non-monotonic dependence would predict the existence of

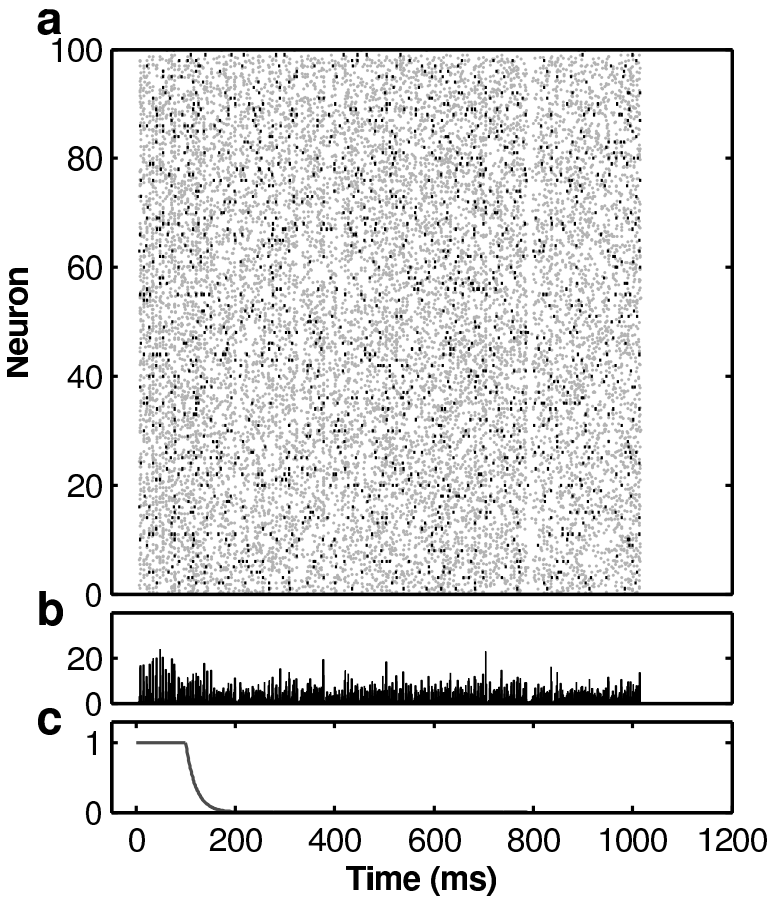

Figure 1.6. Self-sustained activity in conductance based networks (Model 2).
Inducing self-sustained activity in a network comprising $N = 30{,}000$ neurons (see Table 1 for parameters). External input was only necessary to 'ignite' network activity, here we used external inputs firing at a rate of 1 spike/s per neuron. When stationary firing had established itself (here after 100 ms), external input was gradually decreased (exponential decay, time constant 50 ms). Interestingly, the network remained active. In the example shown, self-sustained activity ceased spontaneously after about a second. The small spontaneous 'population burst' that terminated self-sustained activity presumably induced too much inhibition for the network to remain active. *a*, Spiking activity of 100 (black ticks) and 1,000 (gray dots) excitatory neurons randomly selected from the network. *b*, Peri-stimulus time histogram depicting the firing rate (spikes/s) averaged over all neurons in the network (bin size 1 ms). *c*, Temporal protocol for the firing rates (in spikes/s) of the external inputs.

stable self-sustained network activity in the absence of external inputs. Indeed, using a mean field analysis and in network simulations (Kumar et al. 2007) it could be shown that a sufficiently large network with conductance-based synapses, once activated to be in a sufficiently stationary state, shows self-sustained activity without any internal pacemakers, even after all inputs have been removed. The obvious approach to reach this activity state in a network simulation would be to provide external input until all neurons are firing at a rate close to the desired self-consistent rate. The intrinsic stability of this state would then let the network settle at its fixed point, even after switching off the external inputs. Note that the mean firing rate in the network does not decrease, since the reduction in synaptic bombardment received by each individual neuron is fully compensated by an increase in the amplitude of membrane potential fluctuations due to an increased impedance. It turned out, however, that an abrupt change of the input conditions lead to strong transients in the network activity, compromising its stability. To avoid this effect, we used slowly decaying inputs after having reached stationary firing at the fixed point rate (Figure 1.6 c). Under these circumstances, the network remained active for some period of time, even after the external input was completely removed (Figure 1.6 a,b). The population mean of self-sustained activity in the example shown was 13.9 spikes/s. In principle, self-sustained activity can be established also at higher firing rates. For the analysis presented here, however, we concentrated on networks that exhibit AI-type activity at low rates. For an analysis of the survival time of the persistent acitivity and its dependence on network size, synaptic strength, firing rate and synchrony we refer to the original paper (Kumar et al. 2007).

1.3.3 Model 3: Small-scale generic network model of active states

In a third type of model (Model 3), developed at TUG, we simulated neural microciruits in different dynamic regimes in order to analyze their computational properties. With a certain parametrization of the model, we achieved circuit dynamics similar to active states (UP-states). We have simulated the different dynamical characteristics of UP states using circuits of size $3 \times 3 \times 15$ by varying the membrane resistance R_m, the background current $I_{background}$, and the noise current I_{noise} of circuit neurons in parallel.

Circuit models consisted of leaky integrate-and-fire neurons and biologically quite realistic models for dynamic synapses.[1] The membrane voltage V_m of the neuron model was modeled by

$$\tau_m \frac{dV_m}{dt} = -(V_m - V_{resting}) + R_m \cdot (I_{syn}(t) + I_{background} + I_N(t)), \tag{1.10}$$

where $\tau_m = R_m C_m$ is the membrane time constant ($C_m = 5.5$nF; $V_{resting} = -75$mV). Whenever a neuron reaches its threshold of -60mV, a spike is elicited, the membrane potential is set to V_{reset} (chosen for each neuron separately from a uniform distribution between -61.2 and -60.5mV), and clamped there for a refractory period of 2ms. I_{syn} models synaptic inputs from other neurons in the circuits.[2] $I_{background}$ models a constant unspecific background input and I_N models noise in the input. In the simulation, the noise current is implemented by drawing at each simulation time step t a noise current $I_N(t)$ from a normal distribution with mean zero and standard deviation I_{noise}.

Neurons (20% of which were randomly chosen to be inhibitory) were located on the grid points of a 3D grid of dimensions $3 \times 3 \times 15$ with edges of unit length. The probability of a synaptic connection from neuron a to neuron b was $Cexp(-D^2(a,b)/\lambda^2)$, where $D(a,b)$ is the Euclidean distance between a and b, $\lambda = 1.7$ is a spatial connectivity constant, and C is a scaling constant.[3]

For the comparison with experimental data we have used a setting of parameters which defines circuits with dynamics similar to UP-states: Leakage resistance $R_m = 2.74$ MΩ, background current $I_{background} = 6.8$ nA, noise current $I_{noise} = 2.1$ nA. Inputs u to the circuit consisted of four Poisson spike trains, two with a time varying rate r_1 and two with a time varying rate r_2. Every 30 ms, a new rate was drawn from a uniform distribution in the interval $[0, 30]$ Hz for r_1 and r_2 and then kept constant for the next 30 ms. Each input channel was randomly connected to approximately 30% of circuit neurons.

Figure 1.7 shows the spiking activity of neurons and the membrane voltage of a representative excitatory neuron spiking at the mean frequency of about 20 Hz. The neuron shows highly irregular spiking activity. The membrane potential qualitatively matches data from intracellular recordings in UP- and DOWN-states (see, e.g., Anderson et al., 2000; Destexhe et al., 2003; Shu et al., 2003).

[1] Short term synaptic dynamics was modeled according to Markram et al. (1998), with distributions of synaptic parameters U (initial release probability), D (time constant for depression), F (time constant for facilitation) chosen to reflect empirical data (see Maass et al., 2001). The scaling parameters A of the dynamic synapses were chosen randomly from gamma distributions. The mean values (in nA) were chosen to be 15 for projections from excitatory (E) to excitatory neurons, 30 for projections from excitatory to inhibitory (I) neurons, and -9.5 for other connections. In case of input synapses, the A parameter was set to 4.5 (9) for projections to excitatory (inhibitory) synapses. The SD of this parameter was chosen to be 70%. Input synapses were static.

[2] Synaptic inputs are modeled as exponentially decaying currents with a peak current defined by the synaptic weight (which changes over time due to the short term dynamics of synapses), and a time constant of 3ms for excitatory synapses and 6ms for inhibitory synapses.

[3] For connections within the circuit, C was set to 0.1, 0.2, 0.4, and 0.3, for II, IE, EI, and EE synapses respectively. For input connections, C was 0.18 (0.24) for IE (EE) synapses.

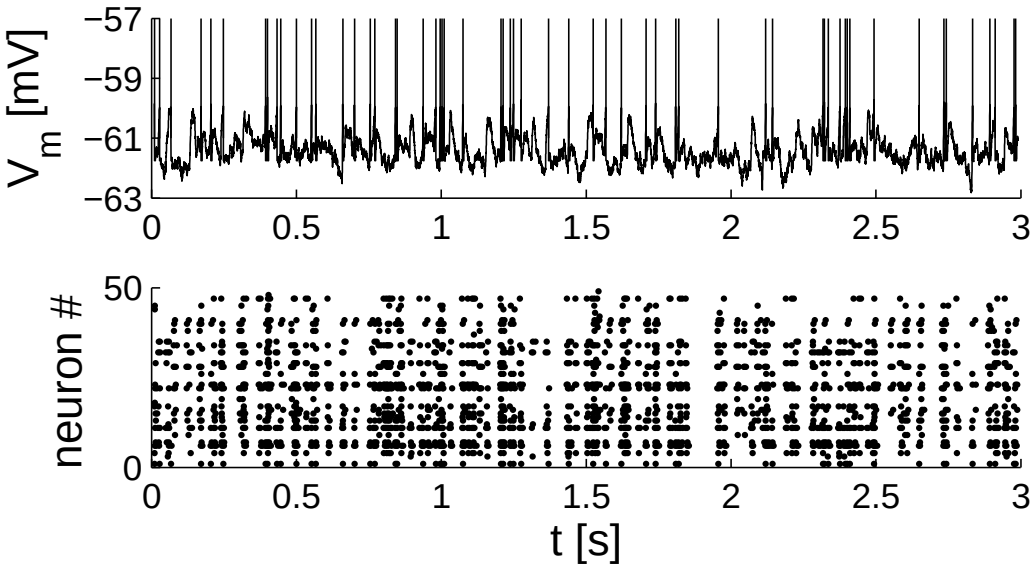

Figure 1.7. Activity of circuit neurons in an active state (Model 3).
Membrane voltage of a neuron in the circuit spiking at 20 Hz (top). Spike rasters of 50 neurons (bottom).

1.3.4 Model 4: Small-scale generic network model of active states

A fourth type of model (Model 4), characterizing a local cortical layer IV circuit in an active state, was developed by UHEI. This model consists of 729 neurons arranged on a 9x9x9 lattice of which 80% and 20% are excitatory and inhibitory neurons, respectively. As physiological data (Braitenberg, 1991) indicates that individual neurons in the cortex receive on the order of 1000-10000 synaptic inputs, one important constraint of the model is that each neuron receives exactly 1000 excitatory and 250 inhibitory synaptic inputs.

Given physiological data on neuron densities and axon cloud distributions (Braitenberg, 1991), it can be inferred that the axon of any given neuron in the local network makes a synapse on only about 20% of the other neurons in the network. The result is that almost 90% of the synaptic inputs to each neuron cannot be supplied by the local simulated network, but must be externally provided.

External activity was provided using inhomogeneous gamma renewal processes (GRP) with two classes of firing statistics (excitatory, inhibitory) consistent with the firing statistics of the simulated neuron model classes (excitatory, inhibitory) provided by such GRP input and with *in-vivo* observations (Destexhe et al., 2003). The unique pair of excitatory and inhibitory Poisson input firing rates which are reproduced by the two classes of simulated neurons was termed the *Model Consistent Background* (MCB) firing rates. The MCB rates represent a fixed point of the network firing rate dynamics. The goal of the work was to determine the criterion for stability of the MCB fixed point, and if a stable fixed point can be found, to compare the observed statistics of the individual neuron firing and conductances in the stable network with biological observations *in-vivo*.

Neuron Model

The IF neuron model as in section 1.2.2 was used, with additional currents of the form

$$g_S(t)(V - E_S) \tag{1.11}$$

$$g_R(t)(V - E_R) \tag{1.12}$$

to account for spike-frequency adaptation (SFA) and a relative refractory (RELREF) mechanism, respectively. When the neuron spikes, the conductances g_S, g_R are increased by q_S, q_R respectively, and are otherwise governed by

$$\frac{d}{dt} g_{\{S,R\}} = -\frac{g_{\{S,R\}}}{\tau_{\{S,R\}}}. \tag{1.13}$$

The neuron model parameters using non-specific units are given in Table 1.1.

Model Consistent Background (MCB) Rates

As already discussed, due to physiological data, almost 90% of the synaptic inputs to each neuron cannot be supplied by the local simulated network, but must be externally provided. External activity was provided using inhomogeneous gamma renewal processes (GRP) with two classes of firing statistics (excitatory, inhibitory)

The unique pair of excitatory and inhibitory Poisson input firing rates which are reproduced by the two classes of simulated neurons (excitatory, inhibitory) was termed the *Model Consistent Background* (MCB) firing rates. The MCB rates represent a fixed point of the network firing rate dynamics.

The MCB rates were determined for the given neuron models by a Monte-Carlo technique: an input rate pair (e, i) for excitatory and inhibitory input rates, respectively was chosen at random and the firing rate of the two neuron classes (f_e, f_i) was determined by simulation. The input rate pair (e, i) was then sought which minimized the quantity $d^2 = (f_e - e)^2 + (f_i - i)^2$. The rough scheme for determining the MCB input rate pair (e, i) is shown in Figure 1.8.

Given the MCB rates, the shape parameter of the gamma renewal process (rate independent) was then determined by fitting the respective ISI distribution of the excitatory and inhibitory neurons supplied with input at the MCB rates. The shape of the input ISI distribution was found to have no significant effect on the firing of the neuron in the case of static input.

Network model

A network model characterizing a local cortical layer IV circuit in an active state was constructed. The model consists of 729 neurons arranged on a 9x9x9 cubic lattice of which 80% and 20% are excitatory and inhibitory

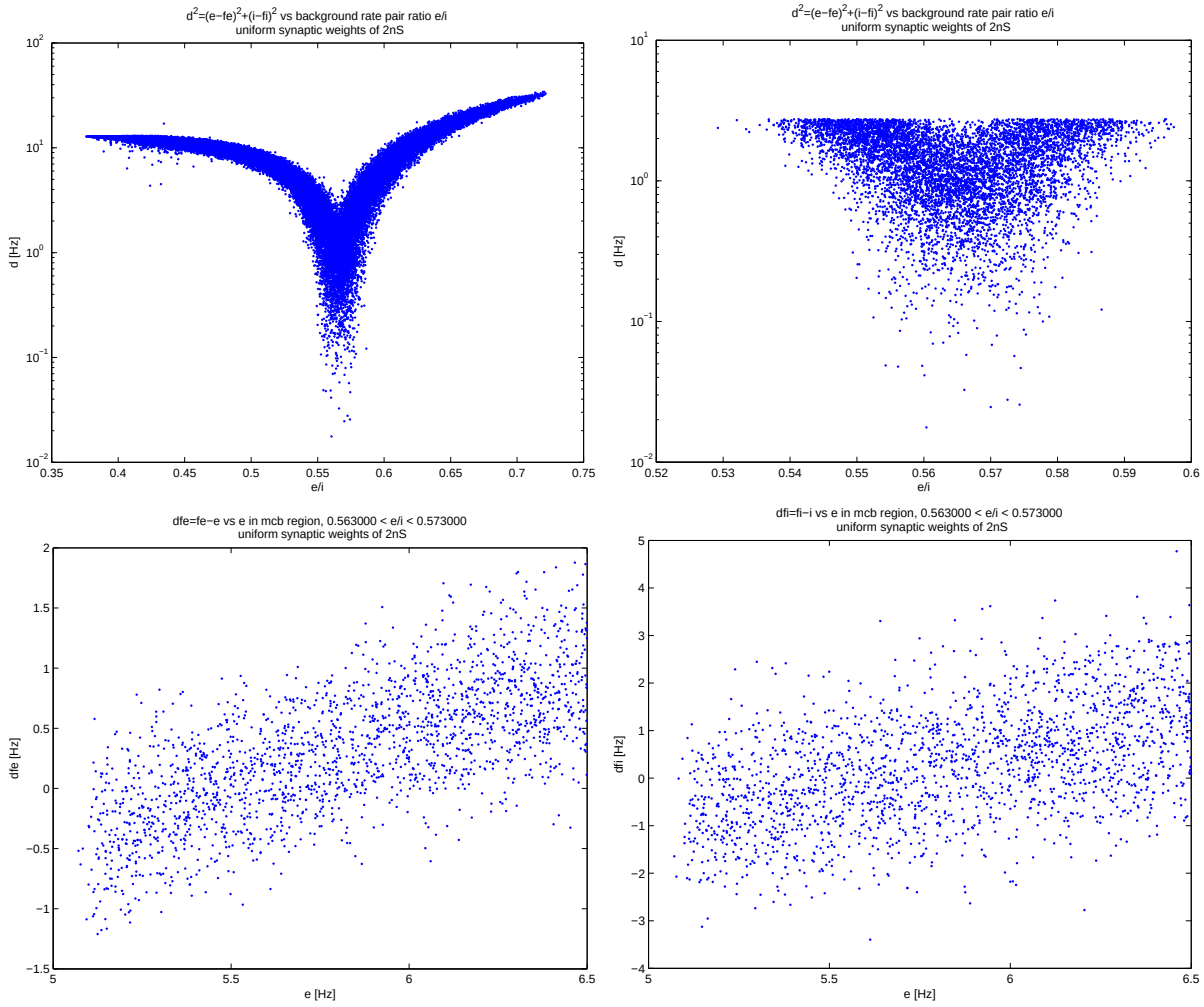

Figure 1.8. Results of Monte-Carlo simulations to determine the Model Consistent Background (MCB) rates (Model 4).
(Top left) The quantity $d^2 = (f_e - e)^2 + (f_i - i)^2$ was found to depend strongly on the ratio e/i. (Top right) The MCB region is revealed to be in on the interval $0.563 < e/i < 0.573$. (Bottom left,right) Given the ratio e/i, it is left to determine either an absolute e or i which has both $df_e = f_e - e$ and $df_i = f_i - i$ simultaneously zero. By inspection it can be seen that $e \approx 5.8$ Hz.

Parameter	Description	Value
V_{TH}	threshold voltage	$-57\,\mathrm{mV}$ (ex), $-54.5\,\mathrm{mV}$ (inh)
V_{RESET}	reset voltage	$-70\,\mathrm{mV}$
C_m	membrane capacitance	$289.5\,\mathrm{pF}$ (ex), $141.0\,\mathrm{pF}$ (inh)
g_L	membrane leak conductance	$28.95\,\mathrm{nS}$ (ex), $21.16\,\mathrm{nS}$ (inh)
E_L	membrane reversal potential	$-70\,\mathrm{mV}$
q_R	RELREF quantal conductance increase	$3214\,\mathrm{nS}$ (ex), $1565\,\mathrm{nS}$ (inh)
τ_R	RELREF conductance decay time	$1.97\,\mathrm{ms}$
E_R	RELREF reversal potential	$-70\,\mathrm{mV}$
q_S	SFA quantal conductance increase	$14.48\,\mathrm{nS}$ (ex), $0.0\,\mathrm{nS}$ (inh)
τ_S	SFA conductance decay time	$110\,\mathrm{ms}$
E_S	SFA reversal potential	$-70\,\mathrm{mV}$
$E_{e,i}$	reversal potential of excitatory and inhibitory synapses, respectively	$0\,\mathrm{mV}$, $-75\,\mathrm{mV}$
$q_{e,i}$	excitatory and inhibitory synaptic quantal conductance increase	$2\,\mathrm{nS}$
$\tau_{e,i}$	excitatory and inhibitory synaptic decay time	$1.5\,\mathrm{ms}$, $10.0\,\mathrm{ms}$

Table 1.1. Neuron and synapse model parameters used for the excitatory (ex) and inhibitory (inh) neuron classes (Model 4).

neurons, respectively. Each neuron receives exactly 1000 excitatory and 250 inhibitory synaptic inputs.

Given physiological data on neuron densities and axon cloud distributions (Braitenberg, 1991), it can be inferred that the axon of any given neuron in the local network makes a synapse on only about 20% of the other neurons in the network. The result is that almost 90% of the synaptic inputs to each neuron cannot be supplied by the local simulated network, but must be externally provided.

Network parameters were calibrated as follows:

- The lattice spacing was calibrated from observed neuron densities on the order of 1×10^5 neurons/mm^3 (Braitenberg, 1991) assuming neurons are on an ordered cubic lattice. The lattice spacing is thus 20 μm.

- Connection delays where determined by the Euclidean distance times a delay factor calibrated to activity propagations speed measurements in Voltage Sensitive Dye recordings *in-vivo* (Petersen et. al., 2003). The delay factor was found to be $0.5\,ms/\mu m$.

- The network represents a $180\,\mu m^3$ volume. Since axon clouds of typical neurons have a radius on the order of $500\,mum$, connection probabilities were uniform in the network.

- The network is too small to consider cortical laminar structure. The model was therefore restricted to a generic local patch of cortical layer IV.

- Connections in the network we parameterized by a set of connection factors ($c_{e\to e}, c_{i\to e}, c_{e\to i}, c_{i\to i}$). Where $c_{e\to i}$ expressed the proportion (on average) of the inhibitory (i) population to which a neuron of the excitatory population (e) is presynaptic in the local network. The various $c_{x\to y}$ were chosen to be around 20% consistent with physiological data (Braitenberg, 1991).

The PyCSIM simulator, a variant of the CSIM neural circuit simulator (`http://www.lsm.tugraz.at/csim`) augmented to run in a distributed environment (MPICH) and allowing configuration and analysis using Python (`www.python.org`) was used for the network simulations described.

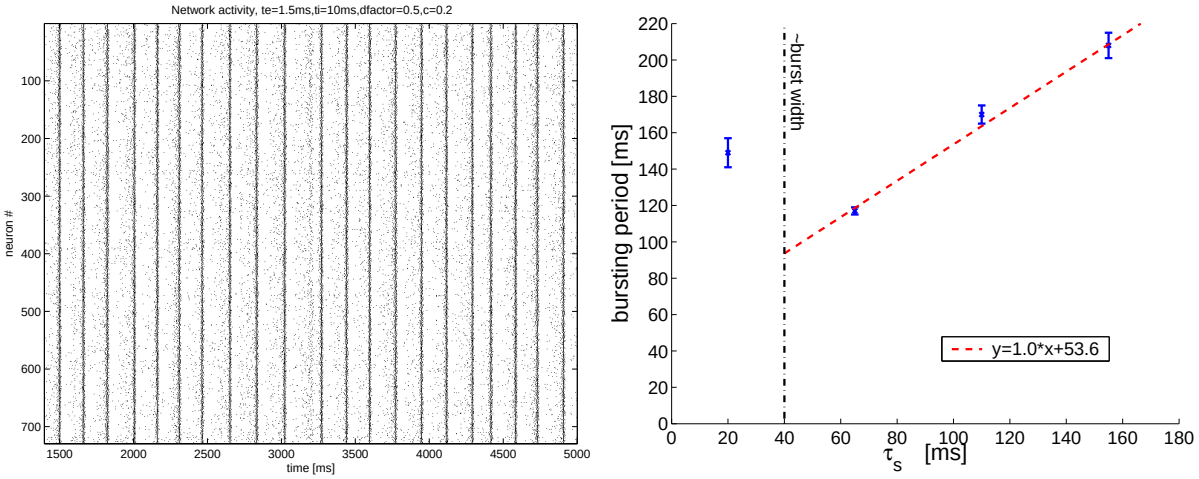

Figure 1.9. Activity of the network (Model 4).
(Left) A raster plot of the spike times for each neuron in the network (connection factors $(0.2, 0.2, 0.2, 0.2)$). The network exhibits marked bursts or synchronizations. (Right) The frequency of these burst was shown to be determined by the time-constant of adaptation.

Preparing the Active Network State

The fixed point of the network activity is known to be the MCB rates by design. It remains to be determined if the fixed point is a stable one. The network was prepared to be at the MCB fixed point by the following scheme:

1. The 729 individual neurons were simulated unconnected (no network) for 500 ms to allow the adaptation and various synaptic conductances to reach equilibrium at the MCB rates.
2. The two neuron classes in the network are thus firing with exactly the firing rates of the external Poisson input they are being driven by, and a fraction of the external synaptic connection can be replaced by connections in the network. The neurons were connected using the prescribed connection factors $(c_{e\to e}, c_{i\to e}, c_{e\to i}, c_{i\to i})$
3. The simulation is resumed for roughly $5 - 10$ s to observe the stability of the MCB fixed point.

Network Activity Stability

First simulations using connections factors $(0.2, 0.2, 0.2, 0.2)$ representing a 20% connected network exhibited epileptic bursting behavior at the frequency of adaptation, as shown in Figure 1.9. Further investigation revealed the MCB fixed point at these connection factors is actually unstable, with diverging network activity kept in check by the accumulation of adaptation.

In the absence of an analytical framework for treating the firing rate of the two conductance-based neurons classes as a function of the input rates, the stability of the MCB fixed point for various connection factors was investigated numerically, by examining the nullclines of the (f_e, f_i) phase plane. Figure 1.10 shows the nullclines for connection factors $(0.2, 0.2, 0.2, 0.2)$. The fixed point at the MCB rates is difficult to resolve due to the uncertainty introduced by finite simulation lengths to determine the firing rate. However, the configuration of the nullclines is clearly that of an unstable fixed point. A slight adjustment of the connection factors to $(0.14, 0.17, 0.2, 0.2)$ results in a stable MCB fixed point, also shown in Figure 1.10. These stable connection factors are subsequently considered for comparison with biological data.

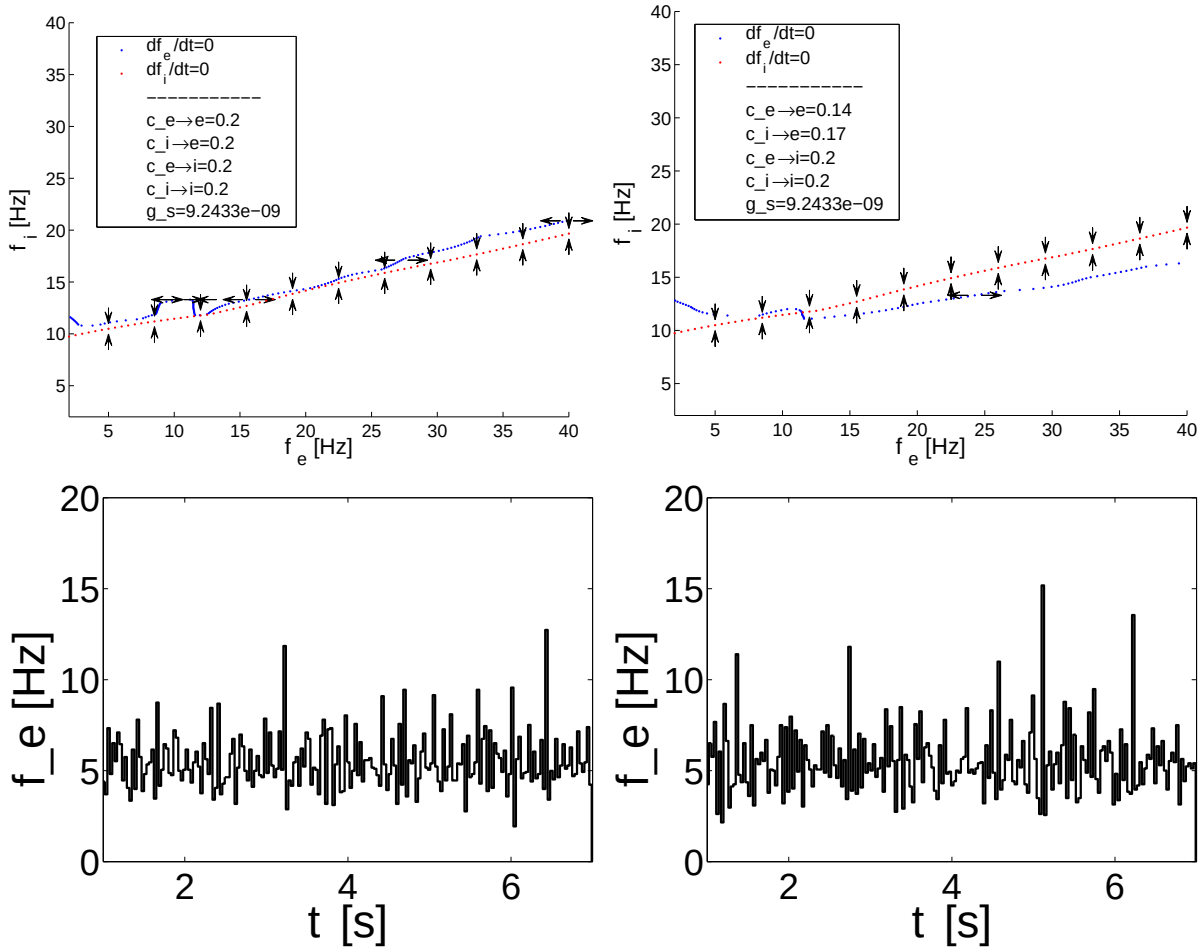

Figure 1.10. Nullclines of Model 4.
(Left) The nullclines of the network firing rates (f_e, f_i) determined by numerical means for connection factors $(0.2, 0.2, 0.2, 0.2)$ (Model 4). The arrows indicate the stability of the respective nullclines. The fixed point at the MCB rates is difficult to resolve due to the uncertainty introduced by finite simulation lengths to determine the firing rate. The configuration of the nullclines is clearly that of an unstable system as the f_e nullcline lies above the f_i nullcline. (Right) The nullclines for connection factors $(0.14, 0.17, 0.2, 0.2)$. The f_i nullcline now lies above the f_e nullcline, and the cross roughly at the MCB rates. As such, the system should oscillate about the fixed point, and further analysis is required to determine if these oscillations are growing or decaying. (Bottom left, right) Typical numerical simulations of networks with these connection factors revealing the network is indeed stable, though it exhibits activity variations larger than an unconnected population.

1.3.5 Model 5: Very-large scale generic network model of local UP states

Finally, a fifth type of approach (Model 5), developed by KTH, consisted of a biophysically detailed model of layer 2/3 of a generic cortical area (Lundqvist et al., 2006). This model has also recently been modified to represent area V1 (see Section 2.3.3 below). This was done in a minimalistic way such as to end up with the functionality of V1 with only minor changes.

The network model includes pyramidal cells and two types of inhibitory interneurons, basket and RSNP cells. These are all modelled with Hodgkin-Huxley dynamics, the pyramidal cells with 6 compartments and the inhibitory interneurons with 3 compartments. Both RSNP and pyramidal cells are of the regularly firing type, while basket cells exhibit fast non-adapting spiking. Model equations and parameters used can be found in Lundqvist et al. (2006) and references therein.

The network model has a minicolumnar as well as a hypercolumnar structure. Each hypercolumn operates like a soft winner-take-all module in which activity is normalized among the minicolumns, such that their summed activity is kept approximately constant. This normalization, which also yields spike synchronization, is achieved through horizontally projecting basket cells. RSNP cells project vertically within a single minicolumn and converts long-range excitatory input to inhibition. The connectivity and EPSPs within a hypercolumn are matched to biological data on PSP magnitudes for different pairs of cell types (Thomson et al., 2002). The global connectivity is constrained also by theoretical considerations, based on activity levels and the total number of synapses on a pyramidal cell.

The represented layer 2/3 portions of a single minicolumn contains 30 pyramidal cells and 2 RSNP cells. The number of minicolumns within a hypercolumn as well as the number of hypercolumns can be subsampled. The model thus contains anywhere between a few thousand and a few million neurons. The behaviour of the network is however maintained through scaling laws of the connectivity. These scaling laws are the result of theoretical calculations based on experimental data of how many active synapses a single cell receives at a given time. This also determines the summed synaptic current received by the postsynaptic neuron. This number is then regarded as a constant, and as the network is scaled the connectivity density is changed to maintain it fixed. In this way we have developed a scalable version of our model that can be simulated on a single PC or on a large cluster (Djurfeldt et al., 2005). We can now easily adjust structure parameters such as the number of minicolumns per hypercolumn, or the total number of hypercolumns in the network. For natural structure parameters, connection probabilities correspond to empirical estimates of cortical connectivity. It is now possible to simulate models of sizeable fractions of brains of small mammals without large sacrifices of model detail. The largest simulation comprised 22 million neurons and 11 billion synapses, corresponding to a cortical surface area of approx. 16 cm^2. This simulation, which was done on an 8 rack Blue Gene/L in collaboration with IBM, is the largest simulations of this type ever performed.

In addition to connectivity constraints there are behavioural constraints on the model. The minicolumns are viewed as the basic computational entities, and the long-range excitatory connectivity in layer 2/3 as storing the memories of the network. The network activity can enter attractor memory states triggered by external stimulation or spontaneously. During retrieval of a memory the network displays attractor activity reminiscent of local UP states (Fig. 1.11, Fig. 1.12). Between 0.5-1% (depending on the number of minicolumns per hypercolumn, 100 or 200) of the pyramidal cells enter this state where they elevate their firing rates to about 10-15 Hz and their soma potential by about 7 mV.

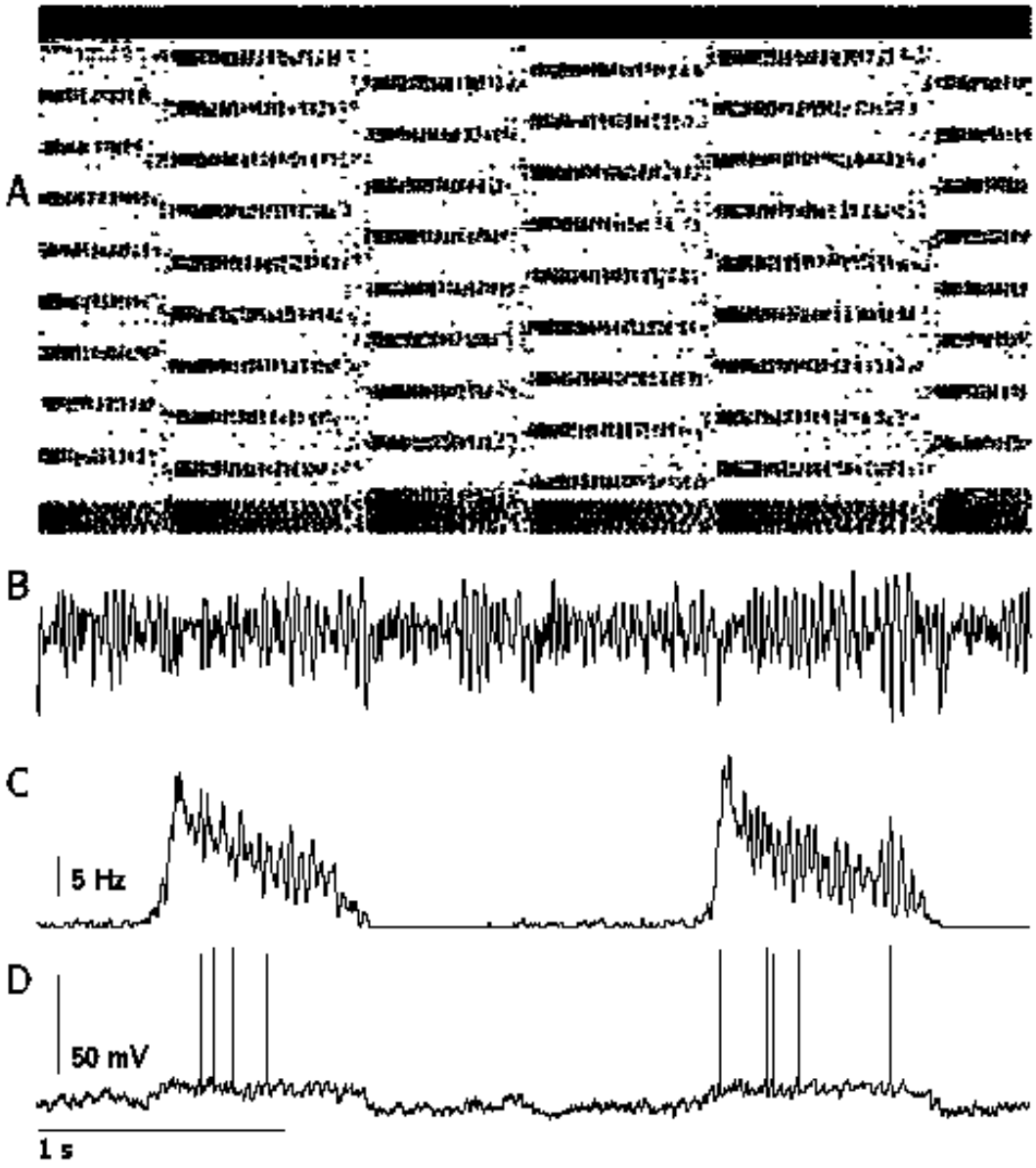

Figure 1.11. Local UP and DOWN states in Model 5.
A. Raster plot of spike activity in the entire network; the topmost, rapidly firing cells are the RSNP cells, then follow the pyramidal cells (sorted by hypercolumn and minicolumn) and finally the basket cells. Simulated time is 4 seconds and different patterns take turns being active, with short transitional periods in between. B. Local field potential; note asynchronous spindles at the UP state onsets. C. Mean spike frequency of the pyramidal cells in one of the patterns, showing UP and DOWN states, the spike frequency being highest at the beginning of UP states. D. Soma potential of one of the pyramidal cells in the same pattern. Membrane potential and spike rate are clearly elevated in the UP state.

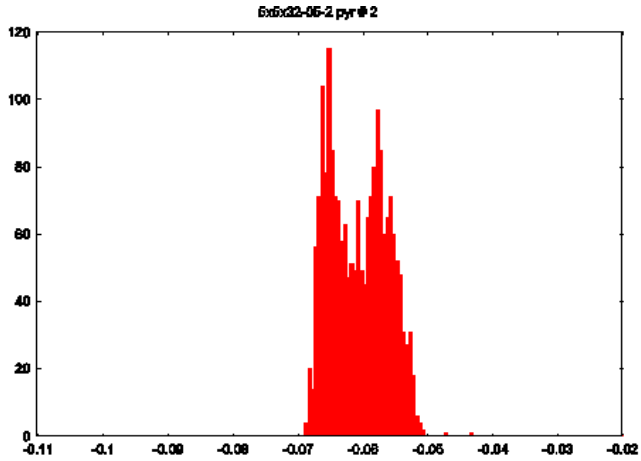

Figure 1.12. Membrane potential histogram for one pyramidal cell during a simulation of 1 s of activity of Model 5 using a network of 25 hypercolumns (100 minicolumns per hypercolumn).
X-axis represents membrane potential in V. Y-axis represents the number of times this potential was attained in a voltage trace binned with a 0.5 ms resolution.? The network spent half of the time in a ground state and half of the time in an UP-state.

1.4 Comparison of generic models to experimental data

1.4.1 Model 1

We analyzed Model 1 similarly to experimental data (see Section 1.1). First, we computed the spontaneous firing rates which were around 15 Hz on average (Fig. 1.13A). This value is similar to the experimental data. However, there was no significant difference between excitatory and inhibitory cells in this model because both cell types were connected similarly. Second, we analyzed the statistics of interspike intervals (ISI), which are exponentially distributed (Fig. 1.13B), exactly as in the data (Fig. 1.2B). Third, we performed a similar avalanche analysis as performed for the experimental data (Bedard et al., 2006). This analysis also failed to evidence power-law scaling behavior but rather indicates exponential distributions (Fig. 1.13C), consistent with the Poisson type dynamics evidenced above. Finally, we estimated the total synaptic conductance in all cells of the network, and displayed the values relative to the leak (Fig. 1.13D). These patterns of conductance revealed a major difference between the model and the experiments: both mean excitatory and inhibitory conductances are significantly stronger in the model compared to the experiments. The difference was particularly strong for inhibitory conductance, which were about 10-fold larger in the model compared to the estimates in real cells.

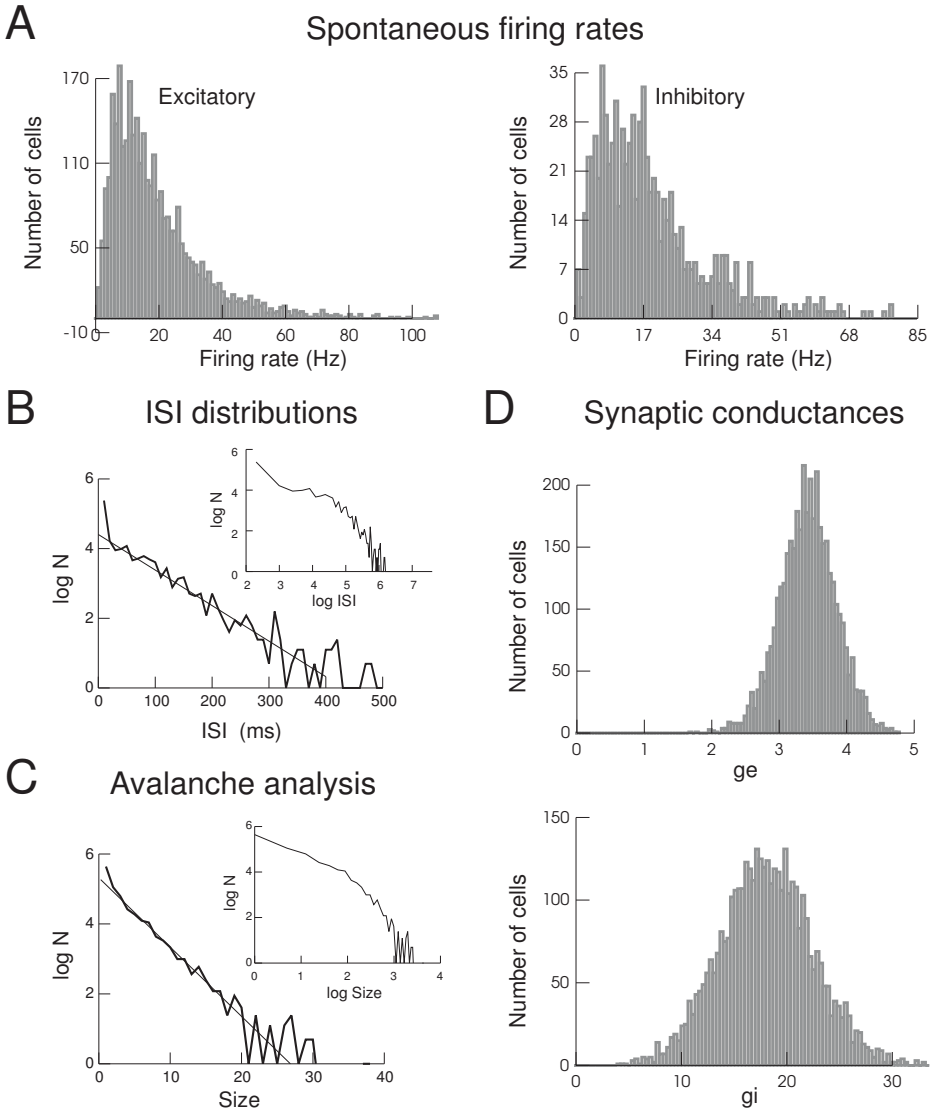

Figure 1.13. Analysis of Model 1 of active states.
A. Distribution of firing rates during the simulated active state. B. ISI distributions are exponential (as for Poisson processes). C. Absence of avalanche dynamics in this model. D. Distribution of relative synaptic conductance values computed from every cell in the network.

1.4.2 Model 2

To characterize the dynamical states of simulated network activity in Model 2, both at the level of single neurons and populations, we employed the following descriptors:

Irregularity of individual spike trains was measured by the squared coefficient of variation of the corresponding inter-spike interval (ISI) distribution

$$\mathsf{CV}^2_{\mathsf{ISI}} = \mathsf{Var}[\mathsf{ISI}] \;/\; \mathsf{E}[\mathsf{ISI}]^2. \tag{1.14}$$

Low values reflect more regular spiking, a clock-like pattern yields $\mathsf{CV}^2_{\mathsf{ISI}} = 0$. On the other hand, $\mathsf{CV}^2_{\mathsf{ISI}} = 1$ indicates Poisson-type behavior. As a measure for irregularity in the network we used the average irregularity across all neurons.

Synchrony for a pair of neurons is typically measured by the correlation coefficient of the joint spike counts C_i and C_j

$$\mathsf{Corr}[C_i, C_j] = \mathsf{Cov}[C_i, C_j] \;/\; \sqrt{\mathsf{Var}[C_i]\;\mathsf{Var}[C_j]}. \tag{1.15}$$

Here, time bins of width 2 ms were used. Note that correlation coefficients may strongly depend on the bin size chosen for analysis (Tetzlaff et al., 2005b). Absolute values of correlation must therefore be carefully interpreted with this caveat in mind. A systematic variation of bin size for various network states showed that for certain network states there is a plateau which guarantees some degree of robustness of the measured values. Also, bins in the range 1–5 ms are commonly used in the experimental literature. As a measure for synchrony of population activity in the network we employed the average correlation coefficient for 250 disjoint pairs of neurons ($\mathrm{CC_S}$).

Using these two measures, network activity can be essentially classified into four different states, as done previously for current based networks (Brunel, 2000). Based on our simulations, we systematically evaluated these statistical descriptors, in addition to firing rate and membrane potential statistics, as a function of the control parameters g and ν_{ext}. The results are shown in Figure 1.14. Note that in our parameter scans different values of g were realized by fixing some value for J_{exc} and varying J_{inh} accordingly. This is not meant to imply that the behavior of the network did not depend on the specific choice of J_{exc} or τ_{exc}, and an independent variation of the strength of excitation and inhibition was performed later.

For low values of inhibition ($g < 1.5$) neurons spiked at high rates and exhibited synchronous activity. Both the firing rate and synchrony increased as the external input was increased (Figure 1.14 a,c). A single frequency dominated the population signal even for asynchronous activity. For large parts of the parameter space, the dominant frequency was between 100 Hz and 200 Hz (data not shown), enclosing the frequency $\frac{1}{4D} = 167$ Hz that is generally expected for a system with a uniform intrinsic delay $D = 1.5$ ms (Murray, 2002; Brunel, 2000; Brunel and Wang, 2003; Maex and De Schutter, 2003; Roxin et al., 2005). Single neuron firing patterns were regular (Figure 1.14 d). The mean free membrane potential was closely below threshold, which was 20 mV above rest (Figure 1.14 e).

As the relative strength of inhibition was increased ($g > 1.5$), the mean membrane potential remained always subthreshold, and firing was driven by fluctuations in the membrane potential. This resulted in quite irregular firing at low rates (< 10 spikes/s). For not to too high values of ν_{ext}, the network generally exhibited asynchronous population activity. In contrast, high synchrony at higher firing rates (> 50 spikes/s) was observed for all values of g in the explored range, if the external input ν_{ext} exceeded 5 spikes/s.

The neurons in all network states observed in our simulations had strongly increased membrane conductances, due to massive synaptic bombardment (Figure 1.14 b). For states that exhibit high network synchrony, the observed values were higher than what is normally found in healthy cortical neurons. AI-type states, in contrast, were accompanied by an increase of the total membrane conductance by a factor 2–5, and a corresponding reduction of the membrane time constant from $\tau_{\mathsf{rest}} = 15$ ms to a value of 3–8 ms. These results are in very good agreement with physiological observations *in vivo* (Destexhe et al., 2003; Leger et al., 2005).

Our results on single-neuron spiking and population activity in networks with conductance based synapses are roughly in line with previous observations in current based networks (Amit and Brunel, 1997; Brunel, 2000; Mehring et al., 2003).

However, we found important differences in the membrane potential statistics of individual neurons during the AI state of the network. In the current based model, the mean membrane potential is often close to the resting potential, while spikes are induced by quite large fluctuations in the membrane potential due to recurrent input. By contrast, in our simulations of networks with conductance based synapses we found that, in the AI state, the mean membrane potential of neurons is only about 5 mV below spike threshold, and the firing is driven by relatively small fluctuations (Figure 1.14 e,f). In fact, the membrane potential of neurons recorded intracellularly

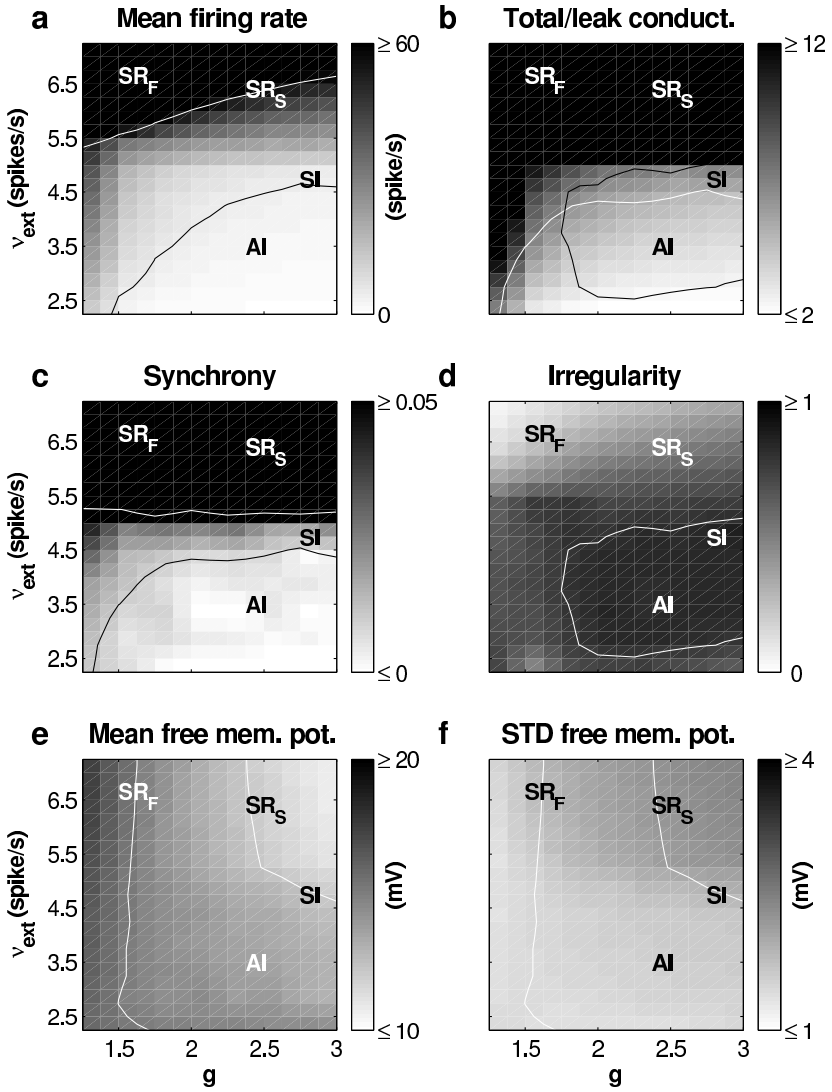

Figure 1.14. Characteristics of network activity in Model 2.
The dynamical states of a large recurrent network (here, $N = 50{,}000$) can be classified by jointly considering several observables, as shown here for different configurations defined by the control parameters g and ν_{ext}. The labels SI, AI, SR_F, and SR_S indicate combinations of parameters which lead to the corresponding network activity. *a*, The neurons in the network fire essentially all at the same rate, shown is the mean across a population of 500 randomly selected neurons. The contour lines correspond to a mean rate of 5 and 60 spikes/s, respectively. *b*, The total conductance of the neuronal membrane is strongly increased relative to the leak conductance ($G_{\text{rest}} = 16.7\,\text{nS}$), for all network states examined here. For AI states, conductances are increased by a factor 2–5, leading to a corresponding reduction of the membrane time constant from $\tau_{\text{rest}} = 15\,\text{ms}$ to a value of 3–8 ms, in accordance with physiological findings. Shown are mean values for a sample of 3 neurons recorded during a network simulation of 1.7 seconds duration. The white contour circumscribes the asynchronous regime (see *c*), the black contour the irregular regime (see *d*). *c*, The level of synchrony in the network (measured by the mean pairwise correlation, see Materials and Methods) was strongly dependent on ν_{ext}, and to some degree also on g. The black contour indicates a value of 0.01, the white contour a value of 0.1 for the synchrony. *d*, The irregularity of the spike trains (measured by the mean normalized variance of the inter-spike intervals, see Materials and Methods), by contrast, was more or less uniform in the inhibition-dominated regime ($g > 1.5$). In the excitation-dominated regime ($g < 1.5$), however, neurons produced quite regular spike patterns. The contours indicates a value of 0.8 for the irregularity. Panels *e* and *f* depict the mean (above rest) and the standard deviation of the free membrane potential, respectively, for a randomly chosen neuron. The contours in both panels are the same, indicating a mean free membrane potential of 12 mV and 15 mV above rest, respectively. The spike threshold was at 20 mV above rest.

in vivo is also close to threshold, and spiking is induced by small fluctuations (Destexhe et al., 2003; Leger et al., 2005). This indicates that the membrane potential dynamics in the current based network model tends to reflect a non-physiological state of the individual model neurons. By contrast, for the conductance based model, both the network dynamics and the membrane potential dynamics are in very good accordance with extracellular and intracellular measurements *in vivo*.

In networks with current based synapses, the transition from high-activity states to low-activity states occurs for a fixed amount of recurrent inhibition at $g_{\mathsf{crit}} = K_{\mathsf{exc}}/K_{\mathsf{inh}}$, independent of external input and network activity. For conductance based networks, by contrast, the transition happens for relatively low values of g, provided the inputs are weak (Figure 1.14 a). For higher values of ν_{ext}, high firing rates (≥ 100 spikes/s) occur in conjuction with high synchrony in the network, and this combination is hardly affected by the amount of recurrent inhibition (Figure 1.14 a,c).

For other aspects of the neuronal and network dynamics (e.g. shape and size of PSPs in active networks, stability of the network dynamics, and the effect of synaptic time constants) we refer to the original paper (Kumar et al. 2007).

1.4.3 Model 3

To analyze the distribution of firing rates in Model 3, we randomly drew 30 circuits with the given parameters and computed the mean number of neurons with a firing rate within intervals of 10 Hz. Since in an experimental setup silent neurons will in general not be detected, we excluded neurons from the analysis which did not generate action potentials at all. The result is shown in Figure 1.15. In accordance with findings in vivo, the distribution of excitatory neurons is approximately exponential with a mean of $13.4Hz$ (here, neurons which do not spike are excluded from the mean. If they are included, the mean drops to $10.7Hz$). The firing rates of inhibitory neurons have a broader distribution with a mean of $32Hz$ (if silent neurons are included, the mean drops to $26.8Hz$).

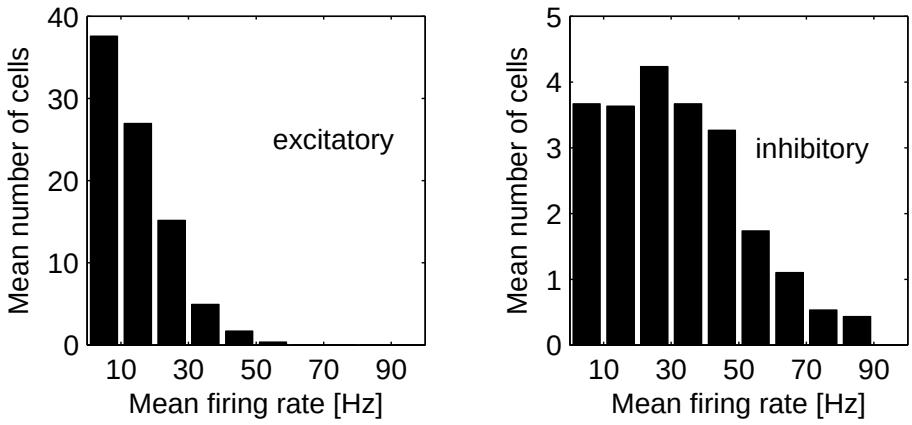

Figure 1.15. Distribution of firing rates of excitatory (left) and inhibitory (right) neurons in Model 3. The approximately exponential distribution of firing rates for excitatory neurons has a mean of 13.4Hz. The distribution of firing rates for inhibitory neurons is broader with a mean of 32Hz.

1.4.4 Model 4

We analyzed the similarity of the MCB stable point network activity to experimental data (see Section 1.1). First, the distribution of average firing rates was computed as shown in Figure 1.16. Second, the average synaptic conductances were computed relative to the leak (only from five cells due to technical limitations) as shown in Figure 1.16. The distributions of both the mean firing rates and mean conductances exhibit less variability than is observed in the biological specimen (see Section 1.1), however the mean of the distributions take on biologically plausible values. Variations in the neuron model parameters, such as the firing threshold, as are observed in the biological specimen, were not modeled and would increase the observed variability. Furthermore, simulations of larger networks could exhibit spontaneous waves of activity which would contribute to further increasing the variability.

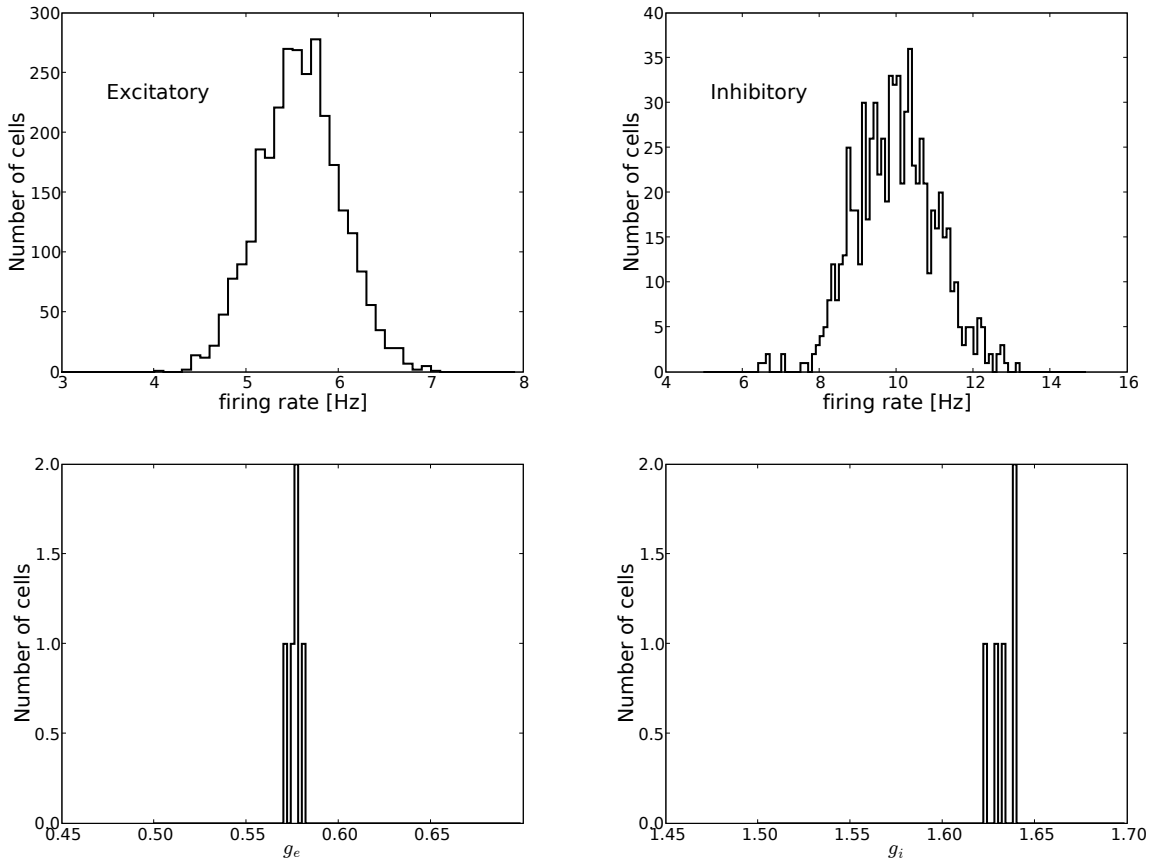

Figure 1.16. (Top row) Distribution of firing rates for both neuron classes in a network at a MCB stable fixed point (Model 4).
(Bottom row) Distribution of mean conductances. Measurements from only five neurons are shown, as presently it was not possible to record the conductances from more neurons in the network.

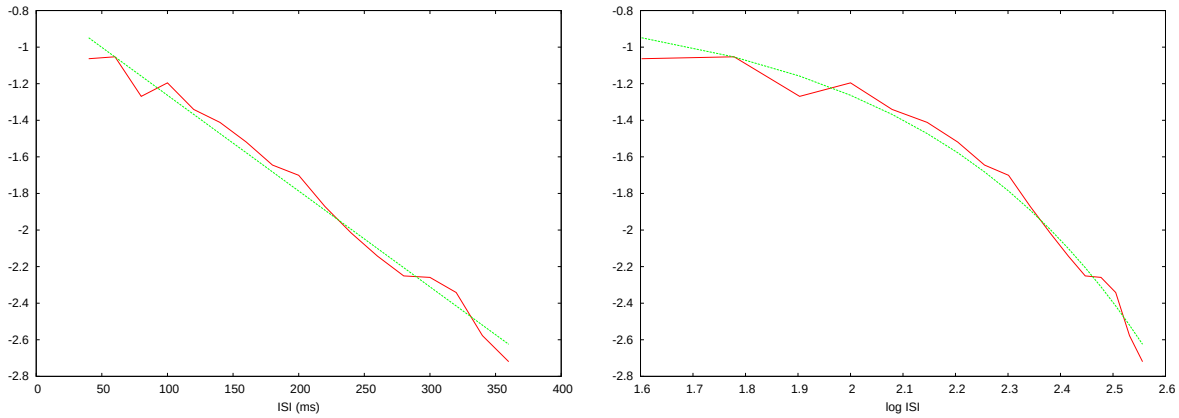

Figure 1.17. Exponentially distributed activity of pyramidal cells in UP-states in a network with 25 hypercolumns (Model 5).
Â Â ISIs: (9443 spikes) were collected from all pyramidal cells during a total of 2 s of simulated time when the network was in an active attractor state, i.e., one in which a subset of cells shows UP-state activity. The logarithm of the distribution of ISI was plotted as a function of (a) ISI length and (b) log ISI length.Â An exponential distribution was fitted to the data and is shown as (a) a straight line and (b) a smooth curve.Â r2 was 0.98 for the exponential fit and 0.86 for a power-law distribution (not shown).

1.4.5 Model 5

The activity of local UP states in Model 5 was analyzed first with respect to ISI distributions. During UP states, the ISI distribution is exponentially distributed (Fig. 1.17) as seen for active states experimentally (see Fig. 1.2B). The UP states last for 500-1000 ms and the rise of soma potential at their onset happens during about 50 ms. When scaling up the size of the model, cortical attractor dynamics was robust to increased axonal propagation delays. In fact, the switch to a new memory state was completed in less than 50 ms even for the largest networks simulated. We further observed more activity in the beginning of the upstates compared to the middle and near the end, as described by Cossart et al. (2003). This change of activity over time in an upstate can be related to the psychological phenomenon called "attentional blink" (Shapiro et al., 1994; Marois and Ivanoff, 2005). The model explains this phenomenon as resulting from that attractors are more stable in the beginning and can thus block incoming stimuli arriving during a certain period after onset.

The distributions of firing rates of the three different cell populations in the network model are plotted in a histogram in Fig. 1.18, and can be compared to Fig. 1.2A. The firing rates for pyramidal cells are given for cells in an upstate only. The mean firing rates as well as distribution and ranges of spike rates of both pyramidal and inhibitory interneurons match experimental data well (10 and 28 Hz respectively).

As cells are modelled with multiple compartments and since the main source of the EEG signal is believed to be currents along the apical dendrites of pyramidal cells, we can recreate such a signal from our model. We use the current entering the soma from the apical dendrite as our source for local field potentials. Looking at the frequency spectrum of such a synthetic EEG produced from spontaneous activity (Fig. 1.11B), the most prominent finding is that of a gamma-like oscillation with a frequency around 25-30 Hz. This signal is almost exclusively generated by negative feedback between pyramidal and basket cells during upstate activity, consistent with experimental data, relating gamma patterns in human EEG to memory matches.

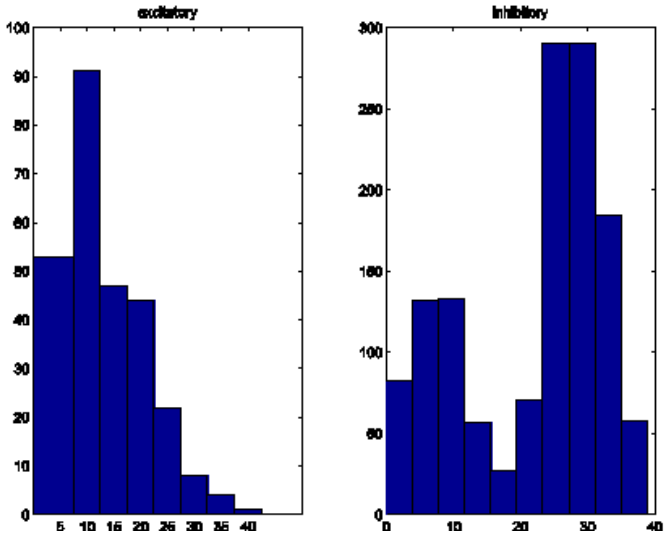

Figure 1.18. Distribution of firing rates for excitatory and inhibitory neurons in Model 5.
The excitatory cell firing rates are from pyramidal cells in an upstate only. For the inhibitory cells both basket and RSNP cells are included. RSNP cells typically fire at higher rates, due to the fact that they are active most of the time.

2

V1 models

In this second part, we report the building of models of primary visual cortex (V1) within FACETS. Only the structure of the models is overviewed here, while the comparison to experimental data will be covered in a specific deliverable (D25).

The models of the early visual pathway used, retina and LGN, will also be described here. They have been set up in a standardized and modular fashion, thus allowing all network models to process exactly the same input and, at the same time, keeping flexibility in the design of these input stages.

2.1 Network models of the retina

INRIA has developed a fairly large simulation platform which is a pure and large-scale event base simulator. This simulator is parameterized by the type of spiking neurons one wishes to simulate and has been implemented very efficiently. Based on this simulator they have developed a spiking retina to be used as input to V1, the originality of the approach being that this model is very close to the biology (Wohrer et al., 2006a).

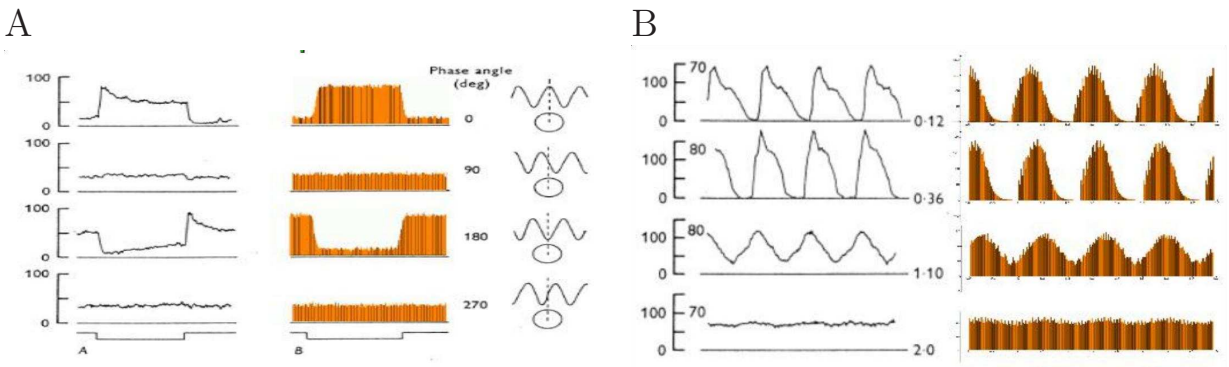

Figure 2.1. Comparison of the retina simulation output with biological experimental results.
A. Trial average firing rates of real (left column, after) and of a simulated (right column) ganglionar off-cell to the reversal of a static grating (experiments from Enroth-Cugell and Robson, 1966). B. Real and simulated cat beta-cell using the same stimulus. Constrast gain control plausibility has also been studied (based on the experiments of Shapley and Victor, 1978).

This artificial retina delivers spikes to higher-level visual task simulations, possibly for large-scale simulations. The architecture of this retina model is based on recent physiological studies, so that each feature is related to real retina characteristics. The model includes a linear filtering process, followed by a static non-linearity, and then a spike generation process. It thus simulates the output of the Parvocellular pathway of primate retinas. Two series of tests were performed: firstly on single cells for which ground truth is available, secondly on realistic visual scenes, taking into account contrast gain control (Wohrer et al., 2006b). An future extension is modeling of the Magnocellular pathway of primate retinas.

2.2 Network models of the thalamus

TUG has developed an LGN model that feeds input into the V1 hypercolumn. The model consists of a realistically dense lattice with 10000 cells that are laid out on a 50 x 50 x 4 grid. The model for the LGN closely follows the standard design (Ferster, 1990; Dong and Atick, 1995, Troyer et al., 1998) and resembles a spatio-temporal filter bank with non-linearities. The filter bank converts time varying input signals from the retina, into firing rates of LGN neurons. Each visual input to the retina evokes four different types of firing rate responses of the retina-LGN model corresponding to the two different types of LGN cells, i.e. of non-lagged or lagged cells, in combination with the two types of retinal cells, i.e. on-center or off-center cells. Lagged and non-lagged LGN cells have been observed experimentally (Mastronarde, 1987; Humphrey and Weller, 1988a; Humphrey and Weller, 1988b). From these firing rates spike trains are generated as LGN output. This standard model was extended by two features. Additional to the short transient high-frequency phasic discharge of LGN cells (in response to a small light spot) a longer lasting tonic discharge was implemented with temporal dynamics taken from CNRS (Gazeres et al., 1998). Secondly, the difference in firing statistics for the initial phasic response and the tonic response was accounted for by implementing a switching gamma renewal process (Gazeres et al., 1998) for the spike generation mechanism.

A network of LGN neurons was also developed at the UNIC in the context of hybrid experiments involving living neurons in real-time interaction with models. For more details on this model, see deliverable D10.

2.3 Network models of V1

At this early stage of FACETS there is not one, but four variant network models of V1 with slightly different characteristics. During the next phase of the project these will be further examined, compared and benchmarked against specific experimental setups. Based on such an evaluation they will be pruned, modified, and refined to arrive at a common FACETS model.

The models have been implemented either with spiking neurons or with more abstract non-spiking units or variables representing the state of a local small subpopulation of neurons. The former have been designed to match closely cellular level biological data, whereas the latter have been kept abstract to allow for analysis of their properties.

In the first part we describe the spiking network models and thereafter a non-spiking one.

2.3.1 A basic spiking model of V1

Recent advances in neurophysiological techniques have greatly increased the knowledge of the cortical neuroanatomy and a quantitative wiring diagram of the local neuronal network of cat visual cortex was described (Binzegger et al., 2004), which provided the first realistic estimate of synaptic connections among various neuron types in different cortical layers. Binzegger specified the total number of neurons in cat area 17 to be $\approx 8.10^7$. The calculation was based on the counted number of cell bodies and synapses in each layer under a square millimeter (Beaulieu and Colonnier, 1983, 1985) and the total surface area of one cortical hemisphere ($\approx 400\ mm^2$ for cat) (Anderson et al., 1988).

CNRS-Marseille has used the data from Beaulieu and Binzegger to specify the neuron numbers and their connectivity in one cubic millimeter of cortex. The resulting network has $\approx 50.10^3$ neurons and $\approx 280.10^6$ synapses. The neurons are distributed on four layers, with each layer having an excitatory and an inhibitory population. The inter- and intra-layer connectivity is drawn randomly, with a connection probability that decreases in a Gaussian fashion with the spatial distance. Fig. 2.2 shows the resulting connectivity of the network. To activate the laminar network it receives non-specifc Poissonian inputs, which are assumed to arise from the surrounding local and distant network.

The intrinsic dynamics of a similar laminar network model were studied in Kremkow et al. (2006). Here we extend the model by adding, to the non-specific Poisson background, specific thalamo-cortical input from the Lateral Geniculate Nucleus (LGN) to layer 4 neurons.

The network is simulated using the NEST simulator (Morrison et al., 2005; NEST). The Python interface (PyNEST) will be used to enable an easier interoperability with the FACETS hardware in a later stage of the project.

The standard leaky integrate-and-fire neuron model is used in the network. Its membrane potential is described

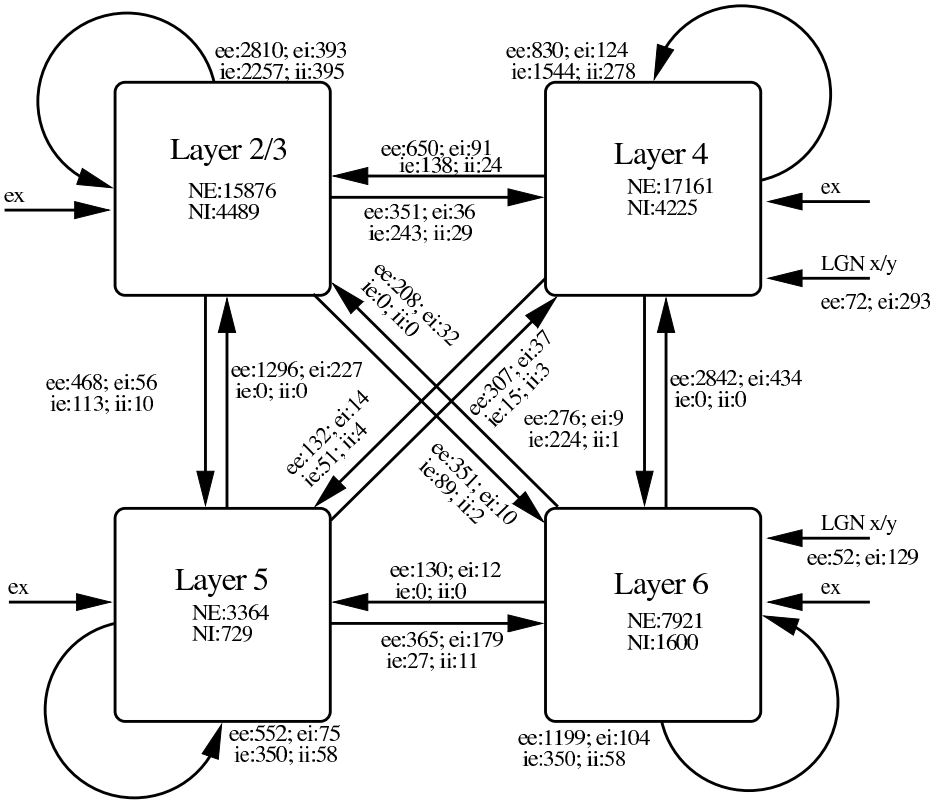

Figure 2.2. Schematic diagram of the V1 network.
NE and NI are the numbers of excitatory and inhibitory neurons, respectively. The labels xy $\{\epsilon\ ee, ei, ie, ii\}$ for each arrow indicate the number of synapses of type x projecting onto a neuron of type y, where e stands for "excitatory" and i for "inhibitory" (adapted from Kremkow et al. 2006).

by:

$$C_m \frac{dV}{dt} = -\sum_{k=e,i,l} G_k(V - E_k) + I_{app} \tag{2.1}$$

here C_m is the membrane capacitance, V membrane potential, G conductance with its reversal potential E of the leak (l), excitatory synapses (e) and inhibitory synapses (i), and I the applied current. The time course of a synaptic conductance transient, e.g. excitatory, after a spike is modeled as a alpha-function

$$\alpha_j(t) = \hat{G}_j^e \frac{t}{\tau_e} e^{-\frac{t}{\tau_e}} \tag{2.2}$$

where j is one particular synapse, $\hat{G}_j^e$ the peak conductance of that synapse and τ_e the time constant.

2.3.2 Addition of short-term plasticity and pinwheel orientation maps

The network model of TUG is based on similar data as above, with additional detail included. The model for a generic cortical circuit (described in deliverable D24) was the starting point. It consists of three layers, with 30%, 20% and 50% of the neurons assigned to layers 2/3, layer 4 and layer 5, respectively. Each layer consists of a population of excitatory neurons and a population of inhibitory neurons with a ratio of 4:1. Connection probabilities and connection strengths between 6 specific populations of neurons (excitatory and inhibitory neurons on layer 2/3, 4 and 5) are chosen according to experimental data assembled by ULON (Thomson et al., 2002). Short term synaptic dynamics is implemented according to EPFL-LNMC (Markram et al., 1998), with synaptic parameters chosen as in a previous study (Maass et al., 2002). Neurons are modelled according to CNRS-Gif-sur-Yvette as conductance based single compartment Hodgkin-Huxley neurons (Destexhe and Pare, 1999; Destexhe et al., 2001). Each neuron receives additional synaptic background noise reflecting the bombardment of synaptic inputs from a large number of more distal neurons which cause a depolarization of the membrane potential and a lower input resistance commonly referred to as "high conductance state".

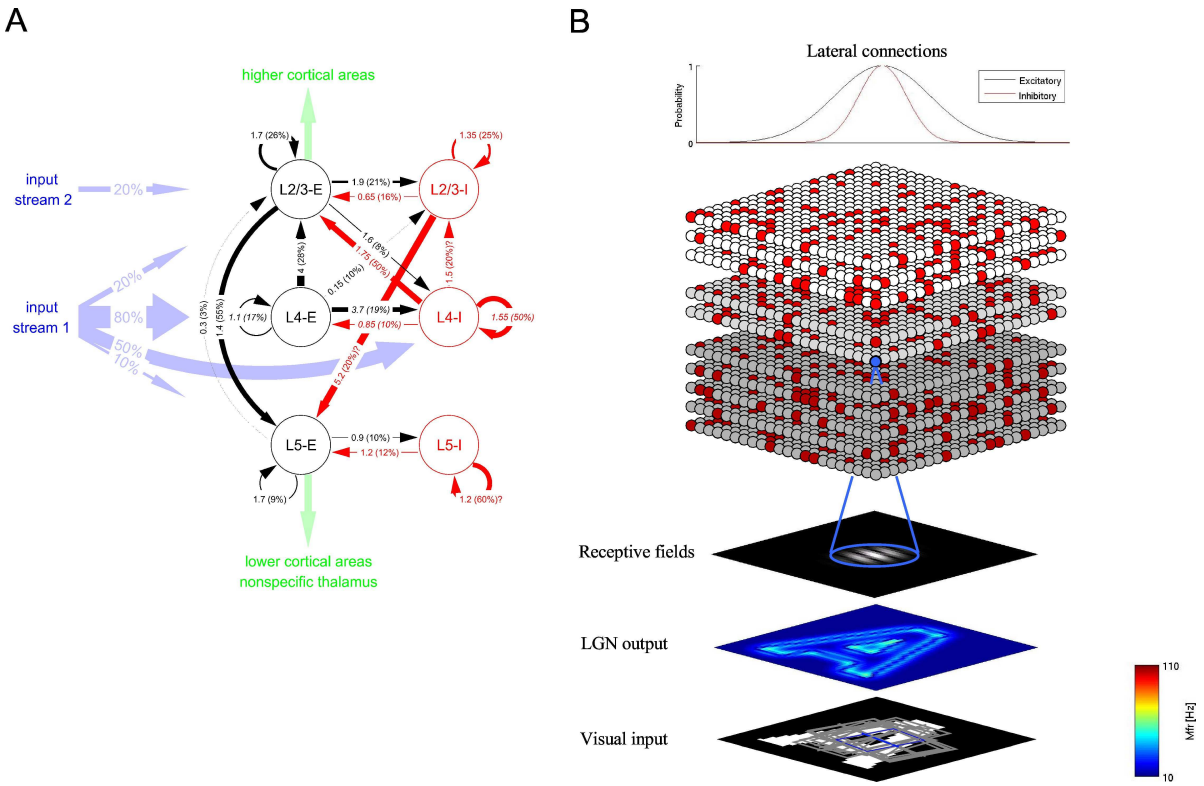

Figure 2.3. Model of a V1 hypercolumn.
A: Generic cortical microcircuit template. Numbers at arrows denote connection strengths (mean amplitude of postsynaptic potentials, PSPs, measured at soma in mV) and connection probabilities (in parentheses) for connections between cortical neurons in 3 different layers, each consisting of an excitatory (E) and an inhibitory (I) population, with an estimated maximal horizontal distance of 100 μm. The experimental data was assembled by ULON (Thomson et al., 2002). B: Extension of the generic circuit model to a V1 hypercolumn by incorporating isotropic and non-specific lateral short range connectivity as found in cat primary visual cortex. Receptive field properties of cortical cells were implemented according to (Troyer et al. 1998) with parameters taken from Teich and Qian (2006).

The above generic cortical circuit model was extended to a model of a V1 hypercolumn by incorporating lateral short range connectivity as found in cat primary visual. In accordance with biological data short-range lateral connectivity is modelled isotropic and non-specific and inhibition acts on a shorter length scale than excitation (Fitzpatrick et al., 1985; Lund, 1987; Callaway and Wiser, 1996; Callaway, 1998). The lateral connection probabilities are modelled by a Gaussian distribution with a standard deviation chosen to be 200 μm and 100 μm for excitatory and inhibitory connections, respectively.

The hypercolumn model consists of 4840 neurons arranged on a 22 x 22 x 10 grid with a lattice spacing of 50 μm. Each unit roughly corresponds to the size of a vertically oriented pyramidal cell module in cat area 17 that is centred on a cluster of apical dendrites from layer 5 pyramidal cells (Peters and Yilmaz, 1993). The inputs from the LGN model are injected mainly into layer 4, into 50% of its inhibitory neurons and 80% of its excitatory neurons, but also into 20% of the excitatory neurons in layer 2/3 and 10% of the excitatory neurons in layer 5. The connection probability between a LGN cell and a V1 cell is modelled according to Troyer et al. (Troyer et al. 1998) by a two-dimensional Gabor function with parameters taken from Teich and Qian (Teich and Qian 2006). The orientation preference of the V1 cells is laid out in the shape of a pinwheel. The spatial frequency for each receptive field is drawn randomly from a Gaussian distribution with mean 0.8 cycles/o and a standard deviation of 0.1 cycles/o (Movshon et al., 1978). The spatial phase preference is taken as uniformly distributed (DeAngelis et al., 1999).

The model is implemented using the neural circuit simulator CSIM (developed by TUG, http://www.lsm.tugraz.at/csim/index.html) in combination with Matlab (for high-level structure and the LGN model). Software tools are ready to run repeated simulations on arbitrary moving image sequences, which are converted to input spike trains to the V1 model by the retina/LGN model described above (Section 2.2). Hence the model can be used for simple in silico experiments, where time-dependent stimuli are shown and spike response

measured. Currently, the lateral extension of the model is enlarged to include several hypercolumns and a larger visual input field. Since one computer will then not be sufficient for performing simulations, the implementation is now ported to the parallel simulator PCSIM (under development at TUG; http://sourceforge.net/projects/pcsim) using python as interpreter language.

2.3.3 Adding self-organized orientation map and learned patchy connectivity

Similar to TUG, the KTH group has modified a generic cortical layers 2/3 model developed previously (Section 1.3.5) into a model of the primary visual cortex. Three separate tasks have been carried out in order to do this. Firstly, a component that models the processes where the cortex receives and recodes signals from the LGN was added. As an initial effort to this end, a model of the cortical layer four was built and connected to the layer 2/3 model. Secondly, the receptive fields of this layer 4 circuitry were generated by a self-organizing and competitive learning process, to reflect the feature maps observed in the visual cortex, such as orientation maps. Thirdly, the layer 2/3 (patchy) horizontal connectivity was generated by training the layer 2/3 on input received from layer 4, using a Hebbian learning rule. The three steps are described further below.

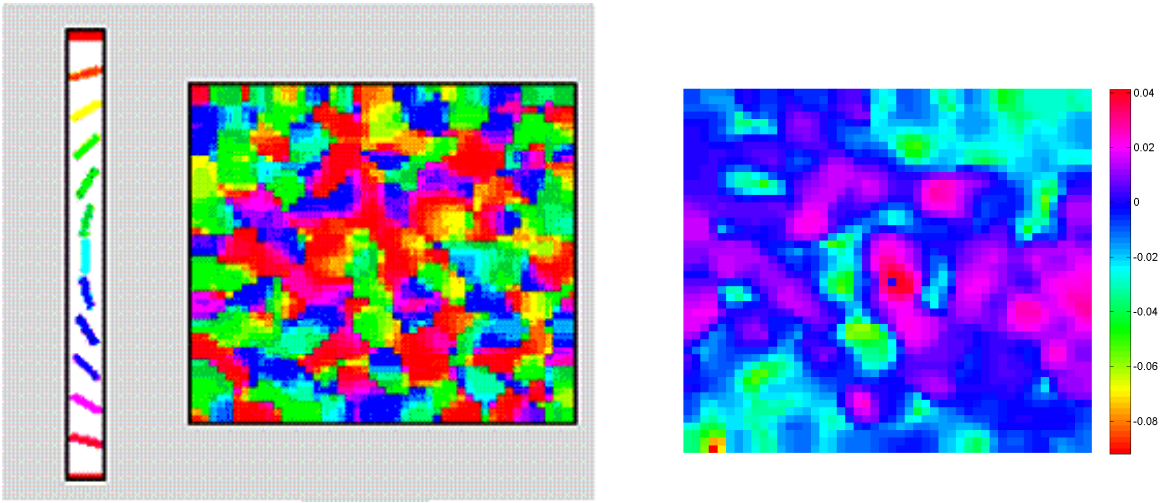

Figure 2.4. Orientation maps in a network model of layer 2/3 of V1.
Left: A 48x48 orientation map generated using the LISSOM program. Right: horizontal patchy connectivity generated by associative learning of activation patterns from lines placed on the orientation map. The connectivity from the minicolumn marked as a dark dot in the central red patch is shown. The basket-cell inhibition is not included.

In order to have a cortical model of the activity response which can be compared directly to experimental observations (using e.g. voltage sensitive dyes) KTH has constructed a variant of the V1 cortex model that exhibits orientation preference maps. This variant borrows part of its circuitry from the LISSOM model, an abstract model which is known to produce orientation preference maps similar to those observed experimentally (Sirosh and Miikkulainen, 1994), see Fig. 2.4 (left) above. The cortical part of this abstract network model is "transplanted" onto the existing layer 2/3 cortical circuitry. The dynamics of the resulting network is compared both to the abstract model and directly to experimental observations. The left figure above shows an orientation map resulting from running the LISSOM model with a size of 48x48 minicolumns, i.e about 2x2 mm).

The final step undertaken in order to transform the generic cortical model into a V1-specific model is to investigate which role Hebbian learning might play in a primary sensory cortical area. The layer four activities generated from the LISSOM network drives a slightly modified version of our previously described cortical layer 2/3 model (Lundqvist et al., 2006; Sandberg et al., 2000). As before, the direct pyramidal-pyramidal connections represent the positive part of the trained connection matrix, whereas the negative part is inverted by the RSNP inhibitory interneurons. The average conduction speed of axons within the modelled cortical patch was set to 0.1 m/s. The only other modification, compared to the previous generic model, consists of making the normalising hypercolumnar structure "fuzzy" rather than crystalline, thus avoiding sharp borders between hypercolumns. The basket cells are now laid out on a regular grid and driven by the surrounding pyramidal cells, as well as providing inhibitory feedback to these. The dependence of connection strengths on distance is in both cases Gaussian.

Figure 2.4 (right) shows the horizontal patchy connectivity generated by generated by associative learning of

activation patterns from lines placed on the orientation map generated by LISSOM/Layer 4. The connectivity from the minicolumn marked as a dark dot in the central red patch is shown. The basket cell inhibition has not been included. Simulation results demonstrate that the network, when trained with stimuli containing line segments, might be capable of performing e.g. contour integration tasks. Also, we will investigate to what extent this model might contribute to contrast invariance of the cortical response, and to the other FACETS benchmarks, as will be reported in D25. Work is ongoing to scale up this cortical patch by about a factor of a hundred and run simulations on the Blue Gene/L recently installed at KTH.

2.3.4 Towards modelling higher level visual processes

The modelling work performed at INRIA is done in the context of visual perception where one is studying such processes as image segmentation, shape from shading, stereo, motion, objects shape representation, learning and recognition. Using their event based simulator, the INRIA group has developed an event-based model of post-V1 structures (MT and IT layers) and validated and experimented with it.

Simulating large networks of spiking neurons is time-consuming but also often intrinsically parallel. The recent advent of powerful and programmable graphic cards seems to be a pertinent solution to the problem: they offer a cheap but efficient possibility to serve as very fast co-processors for the parallel computing that spiking neural networks need. In the context of the network modelling described, INRIA has also investigated how each node of their cluster could be boosted by the addition of a recent Graphical Processing Unit (GPU), in case of a purely event driven simulation, but also in case of a mixed event/time step based approach (Bernhard and Keriven 2006, Chariot, Keriven, Brette 2006). They describe their implementation of three different problems on such a card: two image-segmentation algorithms using spiking neural networks and one multi-purpose spiking neural-network simulator. Using these examples they show the benefits, the challenges and the limits of such an implementation.

INRIA also considers global behaviours and relate the cortical processing to generative modelization of the brain functionalities. Building this link (here not only in the deterministic case but also using stochastic models) allows to define the processing of external inputs and relate the “what’s to be done” to the “how to do it”. The proposed framework consists of defining the perceptual task as an optimization problem, and to derive the corresponding neural network including regularization mechanisms (Touboul and Brette 2006). We have studied in detail the general class of multi-dimensional nonlinear map computations. Using a scalar or vector valued map is an important feature when addressing the modelling of cortical processing units such as cortical columns (Vieville and Kornprobst 2006, Vieville and Rochel 2006). Introducing nonlinear constraints between the map components has several advantages. One is to take noisy measures into account, avoiding statistical bias, and another is to define physical parameters with complex structure (e.g. 3D orientation). In our context, we consider that neural network information is mainly conveyed through spikes, and derive the parameters of the spiking network which implements the formal processing. We are currently considering SRM (Spike Response Model) neurons with piecewise linear kernels and experimenting to understand to which extent neuronal computations such as winner-take-all or nonlinear filtering via anisotropic-adaptive-diffusion are well described in such a context. A step further, if the previous derivation makes sense, this means that we must observe fast adaptive synaptic mechanisms, with respect to the weights, but also fast adaptive mechanisms of delay. This is indeed a recent assumption which has been observed experimentally and which importance for computational models is to be better understood. Both elements are key aspects of the model: they must be confronted with biological facts. This is the next step of this work.

2.3.5 A non-spiking V1 model

UOP has developed and studied a simplified population-based neural field model representing a small patch of visual cortex using two arrays of cells, one excitatory the other inhibitory. Each set of cells is currently arranged in a 50x50 grid, but may be varied, with a cell at position (x, y) representing local activity corresponding to a spatial position on the cortical patch. A synthetic orientation tuning map determines cell tuning and connectivity within the model. In agreement with Bosking et. al. (1997) long range connections from excitatory cells are preferentially made to postsynaptic cells that both have orientation tuning similar to the presynaptic cell and form an axis with it that aligns with its orientation tuning. At shorter distances, connectivity is more indiscriminate in terms of the characteristics of the postsynaptic cell. Axonal propagation delays between cells are distance-dependent in order to induce realistic patterns of spreading activation. Connections from inhibitory neurons are preferentially made using the same criteria; however the range over which they extend is significantly reduced as suggested by Kisvárday et. al. (1997). A leaky integrator continuous response model describes the behaviour of cells. Cells are

defined by

$$\tau_{ct}^{rise} \frac{dV_{ct}^{j}}{dt} = V_{rest} - V_{ct}^{j} + f_{ct}^{j} \tag{2.3}$$

$$\tau_{ct}^{decay} \frac{df_{ct}^{j}}{dt} = -f_{ct}^{j} + \sum_{ct,j} g_i(E_i - V_{ct}^{j}) \ , \tag{2.4}$$

where ct is the cell type (excitatory or inhibitory), τ_{ct}^{rise} is the cell membrane rise time constant of cell type ct, τ_{ct}^{decay} is the cell membrane decay time constant of cell type ct, j is the number of cells of each type, V_{ct}^{j} is the membrane potential of cell j of type ct, V_{rest} is the resting membrane potential, i is the connection type, belonging to the set {AMPA, NMDA, $GABA_A$, $GABA_B$}, and represents the connection types between cells, E_i is the reversal potential of connection type i.

All connections of a particular type, i, between two populations are represented by a single connection. In the spirit of simplicity, this concept is extended further, with all connections of a given type to a population represented by a single input. These grouped inputs are defined by

$$\tau_{i}^{rise} \frac{dg_{i}^{j}}{dt} = -g_{i}^{j} + h_{i}^{j} \tag{2.5}$$

$$\tau_{i}^{decay} \frac{dh_{i}^{j}}{dt} = -h_{i}^{j} + \sum_{k} w_{i}^{a \to b} \ \theta_{t-d_{kj}}^{ct}(V_{ct}^{j}) \ , \tag{2.6}$$

where τ_{i}^{rise} is the rise time constant of connection type i, k are the presynaptic cells to cell j, τ_{i}^{decay} is the decay time constant of connection type i, $w_{i}^{a \to b}$ is the efficacy of connection type i from presynaptic cell type a to postsynaptic cell type b, t is the current time, d_{kj} is the propagation delay from cell k to cell j, $\theta_{p}^{ct}(x)$ is the gain function of x at time p, for cell type ct, and is defined by $\omega^{ct}[x - \phi^{ct}]$, where ϕ^{ct} and ω^{ct} determine the threshold and gain (in spikes per second per millivolt) for cell type ct. This is essentially the rectification model of Carandini and Ferster 2000.

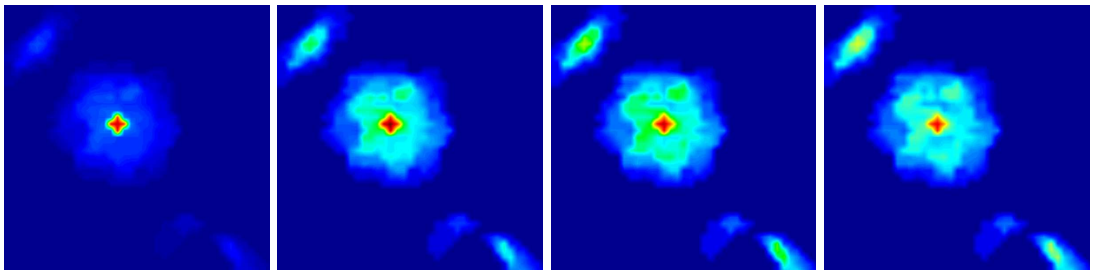

Figure 2.5. Spatiotemporal patterns of activity in a population-based neural field model of V1. Simulated optical signal in the population model showing diffuse local activation and long-range spread of patchy appearance after focal stimulation (red cross).

In the model, focal stimulation positioned at the red area produces similar spatiotemporal activity, as seen in Fig. 2.5 (see e.g. Tucker and Katz (2003) for corresponding optical imaging experimental data). A large, spreading zone of activity is centred on the stimulus site, with two distal zones of activity clearly visible after 17ms. Activation spread follows specific excitatory pathways, but propagation delays induce typical temporal response dispersal. Non-linear effects can contribute to post-synaptic firing according to spatial and temporal summation (not shown).

Conclusions

In this document, we reported on different modeling strategies towards investigating common goals, namely the genesis of active states and the construction of models of primary visual pathways. We summarize below the results obtained, as well as outline future directions that will be followed within FACETS.

2.4 Generic models of active states

In the first part (Section 1), we overviewed experimental data (Section 1.1), single-cell models (Section 1.2) and different network models of active cortical states (Section 1.3). These models range from medium-scale (Model 1, Section 1.3.1) and large-scale networks (Model 2, Section 1.3.2) exhibiting self-sustained active states, small-scale networks exhibiting active states but with external noisy input (Models 3 and 4; Sections 1.3.3 and 1.3.4), and very-large scale networks exhibiting local UP states with attractor dynamics (Model 5; Section 1.3.5). In Section 1.4, we provided comparisons between these models and experimental data, showing that these models reproduce neuronal dynamics consistent with the "active" states in cortex, in particular at the level of distributions of firing rates and collective dynamics. However, conductance dynamics is well reproduced only by some of the models.

It is an unresolved issue, under which conditions real cortical networks share the properties of our models and whether the self-sustained active state is of biological relevance. Nevertheless, experimental evidence pointing in this direction has been reported recently (Shu et al., 2003). A high level of "ongoing" activity without any specific stimulus has also been reported, for example, in the visual cortex (Arieli et al., 1996). Moreover, experiments of "undercutting" cortical tissue to deprive it from input first lead to a silent network, but activity could recur after a few days (Burns and Webb, 1979; Timofeev et al., 2000). Likewise, organotypic cultures of cortical neurons organize into an active network by developing strong enough recurrent synapses (Plenz and Aertsen, 1996).

Having shown that networks of spiking neurons can exhibit self-sustained activity at low firing rates in theory, the question arises which role this particular network state could play for the function of the mammalian neocortex. One possible scenario is that the self-sustained active states provide the functional substrate into which other processes are embedded that eventually subserve higher brain functions. Processes based on spike synchronization (Abeles, 1991; Diesmann et al., 1999; Kumar et al., 2006) could be particularly effective in this context, since they have to merely 'rearrange' the spikes generated by the stable source of ongoing spontaneous activity. This would, among other things, shorten the response times and increase the sensitivity of the processing of inputs. Self-sustained activity in several distinct subnetworks, however, lends itself to the alternative interpretation of short term memory, as proposed by Fuster (1973, 1988), Goldman-Rakic (1995) and others (Compte et al., 2000; Koulakov et al., 2002; Brunel, 2003; McCormick et al., 2003). Also, the possibility to switch between different levels of activity by a very simple 'stimulus' lead to the suggestion (Aertsen et al., 1994; Salinas, 2003) that different contexts of neural processing could be represented by one and the same network in this way. Some of these themes will be explored with FACETS in the future.

After this first generation work is completed, the next step will be to incorporate the diversity of neuronal elements in cortex (diverse firing properties, diverse synaptic interaction) to yield active states fully consistent with the experimental data. In this direction, we will keep the diversity of modeling approaches inherent to FACETS, but integrate now a common type of model (the "FACETS model"), which each group will also develop in parallel. This common model will constitute the "second generation" of models, which will be directly compatible with the hardware.

2.5 Network models of the primary visual pathway

In the second part (Section 2), we have overviewed models of the retina (Section 2.1), of the thalamus (Section 2.2), as well as several models of cortical area V1 (Section 2.3). We refer to the deliverable D25 ("Model for a hypercolumn in V1") for more details on the behavior and biological relevance of these models.

In this case also, these models constitute the "first generation" of FACETS models, in which different groups have pursued largely independent lines of research, resulting in several models of V1, at different levels of detail. The approach of having multiple levels of detail should continue, but it is important now to ensure the compatibility of the different models, and to understand the differences between them where these exist. Therefore, in the second stage of the project, a major effort to compare the assumptions and behavior of the different models is required, in parallel with continuing development of the models. As a key tool to enable this comparison, a library or test-bank of stimulus sets/benchmarks will be built up, beginning by collecting together all the stimuli currently used to test each individual model, and including also the set of stimuli used in biological experiments in WP3. Each model should, where possible, be tested using each benchmark in the test-bank. The results of each model can then be compared to those from all the other models, and to the experimental data that will begin to become available during this stage of the project. For models at the same level of detail (e.g. the spiking models being developed by partners 7 and 6b), efforts will be made to ensure the convergence of the models, such that we obtain a single canonical model (on the scale of a V1 hypercolumn, or larger) at each level of detail. Different groups will then investigate different aspects of the model behavior, and study the effects of variations in the model.

References

Abeles, M. *Corticonics: Neural Circuits of the Cerebral Cortex (1st ed.).* Cambridge: Cambridge University Press, 1991.

Aertsen, A., Erb, M., and Palm, G. Dynamics of functional coupling in the cerebral cortex: an attempt at a model-based interpretation. Physica D 75, 103-128, 1994.

Amit, D. J., and Brunel, N. Model of global spontaneous activity and local structured activity during delay periods in the cerebral cortex. Cereb. Cortex 7, 237-252, 1997.

Anderson, J., Lampl, I., Reichova, I., Carandini, M., Ferster, D. Stimulus dependence of two-state fluctuations of membrane potential in cat visual cortex. *Nat. Neurosci.* **3**: 617-621, 2000.

Anderson, P. A., Olavarria, J., Van Sluyters,R. C. The overall pattern of ocular dominance bands in cat visual cortex.. *J. Neurosci.* **8**: 2183–2200, 1988.

Arieli, A., Sterkin, A., Grinvald, A., and Aertsen, A. Dynamics of ongoing activity: Explanation of the large variability in evoked cortical responses. Science 273(5283), 1868-1871, 1996.

Beaulieu, C., Colonnier, M. The number of neurons in the different laminae of the binocular and monocular regions of area 17 in the cat, Canada. *J. Compar, Neurol.* **217**: 337-344, 1983.

Beaulieu, C., Colonnier, M. A laminar analysis of the number of round-asymmetrical and flat-symmetrical synapses on spines, dendritic trunks, and cell bodies in area 17 of the cat. *J. Compar, Neurol.* **231**: 180-189, 1985.

Bedard, C., Kröger, H. and Destexhe, A. Does the 1/f frequency-scaling of brain signals reflect self-organized critical states ? *Physical Review Letters* **97**: 118102, 2006.

Bernhard F. and R. Keriven, Spiking neurons on GPUs. International Conference on Computational Science. Readings, UK, May 2006.

Binzegger, T., Douglas, R. J., Martin, K. A. C. A quantitative map of the circuit of the cat primary visual cortex. *J. Neurosci.* **39**: 8441-8453, 2004.

Bosking WH, Zhang Y, Schofield B and Fitzpatrick D. Orientation selectivity and the arrangement of horizontal connections in tree shrew striate cortex. *J. Neurosci.* 17: 2112-2127, 1997.

Braitenberg, V., and Schüz, A. Cortex: Statistics and Geometry of Neuronal Connectivity (2nd ed.). Berlin: Springer-Verlag-Verlag, 1998.

Brunel, N. Dynamics of sparsely connected networks of excitatory and inhibitory spiking neurons. J. Comput. Neurosci. 8(3), 183-208, 2000.

Brunel, N. Dynamics and plasticity of stimulus-selective persistent activity in cortical network models. Cereb. Cortex 13(11), 1151-1161, 2003.

Brunel, N., and Wang, X.-J. What determines the frequency of fast network oscillations with irregular neural discharges? I. Synaptic dynamics and excitation-inhibition balance. J. Neurophysiol. 90, 415-430, 2003.

Burns, B. D., and Webb, A. C. The correlation between discharge times of neighbouring neurons in isolated cerebral cortex. Proc. R. Soc. Lond. B. 203(1115), 347-360, 1979.

Callaway, E.M. Local circuits in primary visual cortex of the macaque monkey. *Annu. Rev. Neurosci.* 21: 47-74, 1998.

Callaway, E.M., Wiser, A.K. Contributions of individual layer 2-5 spiny neurons to local circuits in macaque primary visual cortex. *Vis Neurosci* 13: 907-922, 1996.

Carandini M and Ferster D. Membrane Potential and Firing Rate in Cat Primary Visual Cortex. *J. Neurosci.* 20: 470-484, 2000.

Chariot A., R. Keriven, and R. Brette. Simulation rapide de modèles de neurones impulsionnels sur carte graphique, poster at NeuroComp06 conference.

Chiu, C., and Weliky, M. Spontaneous activity in developing ferret visual cortex In Vivo. J. Neurosci. 21, 8906-8914, 2001.

Compte, A., Brunel, N., Goldman-Rakic, P. S., and Wang, X. J. Synaptic mechanisms and network dynamics underlying spatial working memory in a cortical network model. Cereb. Cortex 10(9), 910-923, 2000.

Cossart R, Aronov D, Yuste R. Attractor dynamics of network UP states in the neocortex. *Nature* **423**: 283-238, 2003.

DeAngelis, G.C., Ghose, G.M., Ohzawa, I. and Freeman, R.D. Functional micro-organization of primary visual cortex: receptive field analysis of nearby neurons. *J. Neurosci.* 19: 4046-4064, 1999.

Destexhe, A. and Paré, D. Impact of network activity on the integrative properties of neocortical pyramidal neurons in vivo. *J. Neurophysiol.* 81: 1531-1547, 1999.

Destexhe, A., Contreras, D. and Steriade, M. Spatiotemporal analysis of local field potentials and unit discharges in cat cerebral cortex during natural wake and sleep states. *J. Neurosci.* **19**: 4595-4608, 1999.

Destexhe, A., Rudolph, M., Fellous, J.M. and Sejnowski, T.J. Fluctuating synaptic conductances recreate in vivo-like activity in neocortical neurons. *Neuroscience* 107: 13-24, 2001.

Destexhe, A., Rudolph, M., Paré, D. The high-conductance state of neocortical neurons in vivo. *Nat. Reviews Neurosci.* **4**: 739-751, 2003.

Diesmann, M., Gewaltig, M.-O., and Aertsen, A. Stable propagation of synchronous spiking in cortical neural networks. Nature 402(6761), 529-533, 1999.

Djurfeldt M, Johansson C, Ekeberg 6, Rehn M, Lundqvist M and Lansner A. Massively parallel simulation of brain-scale neuronal network models. Technical Report TRITA-NA-P0513 KTH, School of Computer Science and Communication, Stockholm, 2005.

Dong, D.W. and Atick, J.J. Temporal decorrelation - a theory of lagged and nonlagged responses in the lateral geniculate nucleus. *Network: Computation in Neural Systems* 6: 159-178, 1995.

Enroth-Cugell C and Robson JG. The contrast sensitivity of retinal ganglion cells of the cat. *J. Physiol.* 187: 517-552, 1966.

Ferster, D. X- and Y-mediated synaptic potentials in neurons of areas 17 and 18 of cat visual cortex. *Vis Neurosci* 4: 115-133, 1990.

Fetz, E., Toyama, K., and Smith, W. Synaptic interactions between cortical neurons. In: A. Peters (Ed.), *Cerebral Cortex*, Volume 9, Chapter 1, pp. 1-47. New York and London: Plenum Press, 1991.

Fitzpatrick, D., Lund, J.S. and Blasdel, G.G. Intrinsic connections of macaque striate cortex: afferent and efferent connections of lamina 4C. *J Neurosci* 5: 3329-3349, 1985.

Fuster, J. M. Unit activity in prefrontal cortex during delayed-response performance: neuronal correlates of transient memory. J. Neurophysiol. 36(1), 61-78, 1973.

Fuster, J. M. *The Prefrontal Cortex.* New York: Raven Press, 1988.

Gazeres,N., Borg-Graham, L. J., Frégnac, Y. A phenomenological model of visually evoked spike trains in cat geniculate nonlagged X-cells. *Vis Neuroscience* **15**: 1157-1174, 1998.

Gerstner, W., and Kistler, W. Spiking Neuron Models: Single Neurons, Populations, Plasticity. Cambridge University Press, 2002.

Goldman-Rakic, P. S. Cellular basis of working memory. Neuron 14, 477-485, 1995.

Jack, J. J. B., Noble, D., and Tsien, R. W. *Electric Current Flow in Excitable Cells.* Oxford: Clarendon, 1975.

Hines M. L., Carnevale N. T. The NEURON simulation environment. *Neural Computation* **9**: 1179-1209, 1997.

Humphrey, A.L. and Weller, R.E. Functionally distinct groups of X-cells in the lateral geniculate nucleus of the cat. *J Comp. Neurol.* 268: 429-447, 1988a.

Humphrey, A.L. and Weller, R.E. Structural correlates of functionally distinct X-cells in the lateral geniculate nucleus of the cat. *J Comp. Neurol.* 268: 448-68, 1988b.

Kisvárday ZF, Tóth E, Rausch M and Eysel UT. Orientation-specific relationship between populations of excitatory and inhibitory lateral connections in the visual cortex of the cat. *Cerebral Cortex* 7: 605-618, 1997.

Kornprobst P., T. Vieville, S. Chemla and O. Rochel. Modeling cortical maps with feed-backs European Conference Visual Perception, 2006.

Koulakov, A. A., Raghavachari, S., Kepecs, A., and Lisman, J. E. Model for a robust neural integrator. Nat. Neurosci. 5(8), 775-782, 2002.

Kremkow, J., Kumar, A., Rotter, S., Aertsen, A. Emergence of population synchrony in a layered network of the cat visual cortex. *Neurocomputing*, in press.

Kuhn, A., Aertsen, A., and Rotter, S. Neuronal integration of synaptic input in the fluctuationdriven regime. J. Neurosci. 24(10), 2345-2356, 2004.

Kumar, A., Rotter, S., and Aertsen, A. Propagation of synfire activity in locally connected networks with conductance-based synapses. In Computational and Systems Neuroscience (Cosyne) 2006.

Kumar, A., Schrader, S., Aertsen, A., and Rotter, S. The high-conductance state of cortical networks. Neural Comput., in press, 2007.

Kumar, A., Schrader, S., Rotter, S., and Aertsen, A. Dynamics of random networks of spiking neurons with conductance-based synapses. In: Computational and Systems Neuroscience (Cosyne) 2005, pp. 153, 2005.

Latham, P. E., Richmond, B. J., Nelson, P. G., and Nirenberg, S. Intrinsic dynamics in neuronal networks. I. Theory. J. Neurophysiol. 83, 808-827, 2000a.

Latham, P. E., Richmond, B. J., Nirenberg, S., and Nelson, P. G. Intrinsic dynamics in neuronal networks. II. Experiment. J. Neurophysiol. 83, 828-835, 2000b.

Leger, J., Stern, E., Aertsen, A., and Heck, D. Synaptic integration in rat frontal cortex shaped by network activity. J. Neurophysiol. 1(93), 281-293, 2005.

Lund, J.S. Local circuit neurons of macaque monkey striate cortex: I. Neurons of laminae 4C and 5A. *J Comp Neurol* 257: 60-92, 1987.

Lundqvist M, Rehn M, Djurfeldt M and Lansner A. Attractor dynamics in a modular network model of the neocortex. *Network: Computation in Neural Systems* **17**: 253-276, 2006.

Maass, W., Natschläger, T., Markram, H. Real-time computing without stable states: A new framework for neural computation based on perturbations. *Neural Computation* **14**: 2531-2560, 2002.

Maex, R., and De Schutter, E. Resonant synchronization in heterogeneous networks of inhibitory neurons. J. Neurosci. 23(33), 10503-10514, 2003.

Mastronarde, D.N. Two classes of single-input X-cells in cat lateral geniculate nucleus. I. Receptive-field properties and classification of cells. *J Neurophysiol* 57: 357-380, 1987.

Markram, H., Wang, Y., Tsodyks, M. Differential signaling via the same axon of neocortical pyramidal neurons. *Proc. Natl. Acad. Sci. USA* **95**: 5323-5328, 1998.

Marois, R. and J. Ivanoff. Capacity limits of information processing in the brain. *Trends Cogn. Sci.* **9**: 296-305, 2005.

McCormick, D. A., Shu, Y., Hasenstaub, A., Sanchez-Vives, M., Badoual, M., and Bal, T. Persistent cortical activity: mechanisms of generation and effects on neuronal excitability. Cereb. Cortex 13(11), 1219-1231, 2003.

Mehring, C., Hehl, U., Kubo, M., Diesmann, M., and Aertsen, A. Activity dynamics and propagation of synchronous spiking in locally connected random networks. Biol. Cybern. 88(5), 395-408, 2003.

Morrison, A., Mehring, C., Geisel, T., Aertsen, A., Diesmann, M. (2005) Advancing the boundaries of high-connectivity network simulation with distributed computing. *Neural Computation* **17**: 1776-1801, 2005.

Movshon, J.A., Thompson, I.D. and Tolhurst, D.J. Spatial and temporal contrast sensitivity of neurones in areas 17 and 18 of the cat's visual cortex. *J Physiol* 283: 101-120, 1978.

Murray, J. D. *Mathematical Biology. I: An Introduction* (3rd ed.). Berlin: Springer, 2002.

Plenz, D., and Aertsen, A. Neural dynamics in cortex-striatum co-cultures II - spatiotemporal characteristics of neuronal activity. Neuroscience 70(4), 893-924, 1996.

NEST: www.nest-initiative.org

Peters, A. and Yilmaz, E. Neuronal organization in area 17 of cat visual cortex. *Cereb Cortex* 3: 49-68, 1993.

Rauch, A.and La Camera, G., Lüscher, H., Senn, W., and Fusi, S. Neocortical pyramidal cells respond as integrate-and-fire neurons to in vivo like input currents. J. Neurophysiol. 90, 1598-1612, 2003.

Rotter, S., and Diesmann, M. Exact digital simulation of time-invariant linear systems with applications to neuronal modeling. Biol. Cybern. 81(5/6), 381-402, 1999.

Roxin, A., Brunel, N., and Hansel, D. The role of delays in shaping spatio-temporal dynamics of neuronal activity in large networks. Phys. Rev. Lett. 94(23), 238103, 2005.

Rudolph, M., Pospischil, M., Timofeev, I. and Destexhe, A. Inhibition determines membrane potential dynamics and controls action potential generation in awake and sleeping cat cortex. *J. Neurosci.* (under review), 2007.

Salinas, E. Background synaptic activity as a switch between dynamic states in network. Neural Comput. 15, 1439-1475, 2003.

Sandberg A, Lansner A, Petersson KM and Ekeberg O. Bayesian attractor networks with incremental learning. *Network: Computation in neural systems* 13: 179-194, 2002.

Schrader, S., Kumar, A., Rotter, S., and Aertsen, A. Dynamics of self-sustained activity. In Proceedings of the 30th Göttingen Neurobiology Conference, 2005.

Shapiro, K. L., J. E. Raymond and K. M. Arnell Attention to visual pattern information produces the attentional blink in rapid serial visual presentation. *J. Exp. Psychol. Hum. Percept. Perform.* **20**: 357-371, 1994.

Shapley R and Victor JD. The contrast gain control of the cat retina. *Vision Res.* 19: 431-434, 1979.

Shu, Y., Hasenstaub, A., and McCormick, D. A. Turning on and off recurrent balanced cortical activity. Nature 423(6937), 288-293, 2003.

Shu, Y., Hasenstaub, A., Badoual, M., Bal, T., McCormick, D.A. Barrages of synaptic activity control the gain and sensitivity of cortical neurons. *J. Neurosci.* **23**: 10388-10401, 2003.

Sirosh J, Miikkulainen, R. Cooperative Self-Organization Of Afferent And Lateral Connections In Cortical Maps. *Biological Cybernetics* 71: 66-78, 1994.

Steriade, M., Timofeev, I., Grenier, F. Natural waking and sleep states: a view from inside neocortical neurons. *J. Neurophysiol.* **85**: 1969-1985, 2001.

Teich, A.F. and Qian, N. Comparison among some models of orientation selectivity. *J Neurophysiol* 96: 404-419, 2006.

Tetzlaff, T., Aertsen, A., and Diesmann, M. Time-scale dependence of inter-neuronal spike correlations. In Proceedings of the 30th GÂ¨ottingen Neurobiology Conference, 2005.

Thomson AM, West DC, Wang Y, Bannister AP. Synaptic connections and small circuits involving excitatory and inhibitory neurons in layer 2-5 of adult rat and cat neocortex: Triple intracellular recordings and biocytin labelling in vitro. *Cerebral Cortex* **12**:936-953, 2002.

Timofeev, I., Grenier, F., Bazhenov, M., Sejnowski, T. J., and Steriade, M. Origin of slow cortical oscillations in deafferented cortical slabs. Cereb. Cortex 10(12), 1185-1199, 2000.

Touboul J., R. Brette : Dynamics of noisy inhibitory networks of integrate-and-re neurons: a stochastic network theory approach, poster at Neuromath06.

Troyer, T.W., Krukowski, A.E., Priebe, N.J. and Miller, K.D. Contrast-invariant orientation tuning in cat visual cortex: thalamocortical input tuning and correlation-based intracortical connectivity. *J Neurosci* 18: 5908-5927, 1998.

Tucker TR and Katz CK. Spatiotemporal patterns of excitation and inhibition evoked by the horizontal network in layer 2/3 of ferret visual cortex. *J. Neurophysiol.* 89: 488-500, 2003.

Tuckwell, H. C. *Introduction to Theoretical Neurobiology, Volume 1.* Cambridge: Cambridge University Press, 1988a.

Tuckwell, H. C. *Introduction to Theoretical Neurobiology, Volume 2.* Cambridge: Cambridge University Press, 1988b.

Vieville T. and P. Kornprobst. Modeling Cortical Maps with Feed-Backs, Int. J. Conf. Neural Networks 2006 and Int. Conf. on Cognitive and Neural Systems 2006.

Vieville T. and O. Rochel, One step towards an abstract view of computation in spiking neural-networks, Int. Conf. on Cognitive and Neural Systems.

Vogels TP, Abbott LF. Signal propagation and logic gating in networks of integrate-and-fire neurons. *J. Neurosci.* **25**: 10786-10795, 2005.

Wohrer A, Kornprobst P and Vieville T. From Light to Spikes: a large-scale Retina simulator. IJCNN: International Joint Conference on Neural Networks 2006a.

Wohrer A, Kornprobst P and Vieville T. Contrast Gain Control through a Feedback in the Retina. NeuroComp 2006 conference, 2006b.